The Journal of Chemical Physics

# The effect of collisions on the rotational angular momentum of diatomic molecules studied using polarized light

Cite as: J. Chem. Phys. **153**, 184310 (2020); https://doi.org/10.1063/5.0024380
Submitted: 07 August 2020 . Accepted: 20 October 2020 . Published Online: 12 November 2020

P. T. Arndt, J. Huennekens, C. Packard, V. Tran, J. Carey, R. Livingston, V. M. Marcune, B. A. Rowe, J. Ng, J. Qi, A. M. Lyyra, and E. H. Ahmed

The Journal of Chemical Physics

# The effect of collisions on the rotational angular momentum of diatomic molecules studied using polarized light

Cite as: J. Chem. Phys. **153**, 184310 (2020); https://doi.org/10.1063/5.0024380
Submitted: 07 August 2020 . Accepted: 20 October 2020 . Published Online: 12 November 2020

P. T. Arndt, J. Huennekens, C. Packard, V. Tran, J. Carey, R. Livingston, V. M. Marcune, B. A. Rowe, J. Ng, J. Qi, A. M. Lyyra, and E. H. Ahmed

The Journal of Chemical Physics ARTICLE scitation.org/journal/jcp

# The effect of collisions on the rotational angular momentum of diatomic molecules studied using polarized light

Cite as: J. Chem. Phys. 153, 184310 (2020); doi: 10.1063/5.0024380
Submitted: 7 August 2020 • Accepted: 20 October 2020 •
Published Online: 12 November 2020



P. T. Arndt,[1] J. Huennekens,[2] C. Packard,[1] V. Tran,[1] J. Carey,[1] R. Livingston,[1] V. M. Marcune,[1] B. A. Rowe,[1] J. Ng,[1] J. Qi,[3] A. M. Lyyra,[1] and E. H. Ahmed[1,a)]

## AFFILIATIONS

[1]Physics Department, Temple University, Philadelphia, Pennsylvania 19122, USA
[2]Physics Department, Lehigh University, Bethlehem, Pennsylvania 18015, USA
[3]Department of Physics and Astronomy, Penn State University, Berks Campus, Reading, Pennsylvania 19610, USA

[a)]**Author to whom correspondence should be addressed:** erahmed@temple.edu

## ABSTRACT

We report results of an experimental study of the changes in the alignment of the rotational angular momentum of diatomic molecules during elastic collisions. The experiment involved collisions of diatomic lithium molecules in the $A^1\Sigma_u^+$ excited electronic state with noble gas atoms (helium and argon) in a thermal gas phase sample. Polarized light for excitation was combined with the detection of polarization-specific fluorescence in order to achieve magnetic sublevel state selectivity. We also report results for rotationally inelastic collisions of $Li_2$ in the lowest lying rotational levels of the $A^1\Sigma_u^+(v = 5)$ vibrational state with noble gas atoms.



## I. INTRODUCTION

Understanding the underlying mechanisms of atom–molecule collisional processes is of fundamental importance for many research areas including chemical reactivity, ultracold atoms and molecules, and astrophysics of the interstellar medium. In addition, collision-induced satellite lines can be used to expand the size of datasets in spectroscopic studies of molecules.[1–5] In general, molecules are not spherically symmetric objects, and as a result, most collisional processes involving them depend strongly on the relative alignment of the colliding partners. One of the simplest cases of atom–molecule collisions involves homonuclear diatomic molecules and noble gas atoms. Such systems have been used in numerous experiments that have mostly focused on inelastic collisions in which the rotational and/or vibrational state of the molecule changes.[4–40] Many of these experiments were carried out with the lighter alkali dimers $Li_2$[4–18] and $Na_2$[19–23] due to their relatively simple electronic structure and the convenient transition wavelengths for laser excitation in the visible and near IR regions. Examples of other homonuclear as well as heteronuclear diatomic molecules that were used in such studies include $I_2$,[24–26] $Br_2$,[27,28] $N_2$,[29] NaLi,[30] NaK,[31–33] NaCs,[33] CsF,[34] and BaO,[40] among others. Theoretical studies of rotationally inelastic collisions have also been carried out,[41–48] and good agreement between calculated and measured cross sections was obtained for the $Li_2\left(A^1\Sigma_u^+\right)$ – Ne system by Alexander and Werner[44] and for $NaK\left(A^1\Sigma^+\right)$ – He, Ar by Price and Hickman.[33,46–48]

In this work, we focus on changes in the alignment of the rotational angular momentum $\vec{N}$ during elastic collisions. The angular momentum coupling case that applies to $Li_2$ in the $A^1\Sigma_u^+$ excited electronic state is Hund's case (b). In case (b), the orbital angular momentum vector $\vec{L}$ precesses rapidly around the internuclear axis so that only its projection, $\Lambda$, onto that axis remains relevant.[49] In the present case, $\Lambda = 0$ and $S = 0$, and when the nuclear spin is excluded, the total angular momentum of the molecule $\vec{J} = \vec{L} + \vec{S} + \vec{N}$ reduces to the nuclear rotational angular momentum, $\vec{N}$, of the molecule ($\vec{J} = \vec{N}$). Therefore, the state selectivity provided by the electric

dipole selection rules[49] for the total angular momentum, $\vec{J}$, applies directly to the rotational angular momentum, $\vec{N}$, during transitions. In addition, dipole selection rules for the projections ($M$) of $\vec{J}$ or $\vec{N}$ onto the space fixed $z$ axis facilitate our ability to probe the alignment of the rotational angular momentum (plane of rotation) of the molecule. In comparison to $J$-changing collisions, $M$-changing collisions have been studied less, and as a result, the existing results are somewhat inconsistent. In early work described in Refs. 25 and 26, it was concluded that $M$ is conserved for elastic collisions and that the changes in $M$ obey $\Delta M < \Delta J$ for inelastic collisions.[8] Then, Silvers *et al.*,[50] in experiments investigating BaO in a $J = 1$ state, concluded that elastic collisions with argon preserve $M$ ($\Delta M = 0$), while elastic collisions with $CO_2$ often resulted in changes in $M$. Furthermore, other experiments employing different techniques and molecules (CsF,[34] NO,[51] CO,[52] and others) reported $M$-changing elastic and inelastic collisions. Alexander and Davis[45] reported theoretical calculations that provide further insights into the nature of $M$ changes in rotationally inelastic collisions. One of the principal motivations for the current work is to fill some gaps in the understanding of these phenomena.

Most of the earlier experiments involved the measurement of the net depolarization of the emitted fluorescence due to collisions that rearrange populations within an $M$ manifold of a rotational level.[7,8,25,26,53,54] Such measurements were typically carried out with circularly polarized single laser excitation and consecutive detection of polarized fluorescence. Shortcomings that plagued some of these works included the lack of final state selectivity[53] and the preparation of multiple initial $J$ levels.[25,26,53] Rowe and McCaffery used measurements of fluorescence depolarization to determine cross sections for transfer of orientation in elastic[7] and inelastic collisions[8] of $Li_2(A^1\Sigma_u^+)$ molecules with helium atoms. However, in these experiments, the lithium density was sufficiently high that depolarization due to lithium collisions was probably also significant. Similarly, Wolfe *et al.*[32] and Jones *et al.*[33] used polarization spectroscopy to determine the fraction of orientation lost in NaK inelastic $J$-changing collisions with noble gas atoms. However, because the initial $J$ values used in these experiments ranged from 14 to 44, this technique also did not provide information on specific $M$ to $M'$ transitions.

In contrast to these results, the double resonance excitation experiment of Silvers *et al.*,[50] with BaO in a $J = 1$ level, made a simple interpretation of the results possible. These authors prepared a sample of molecules in $J = 1$, $M = 0$ sublevel by pumping a $^1\Sigma(J = 1) \leftarrow {}^1\Sigma(J = 0)$ transition with linearly polarized light. They then probed a $^1\Sigma(J = 0) \leftarrow {}^1\Sigma(J = 1)$ transition with light that was polarized either parallel to or perpendicular to the pump laser polarization. In the former case, only molecules in the directly excited $M = 0$ sublevel were sampled, while in the latter case, only molecules in the collisionally excited $M = \pm 1$ sublevels were sampled. In addition, in this double resonance experiment using narrow bandwidth lasers, levels with very low $J$ values were selectively probed. This is not possible with single laser excitation. In such experiments, the Doppler broadening in a thermal sample leads to excitation of several levels with similar $J$ values close to the band origin. Silvers *et al.* were unable to detect any changes in $M$ for elastic collisions of BaO with argon (and thus could only place an upper limit to the cross section) but were able to determine a cross section of $4.2 \pm 1.2$ Å$^2$ for similar collisions with $CO_2$.

In our experiments, we use a system consisting of diatomic lithium molecules colliding with noble gas atoms (helium and argon) in a thermal gas phase environment. Our main goal is to study elastic $M$-changing collisions within a rotational level. For this, the molecules are first prepared in a specific ($J$, $M$) initial state. We have chosen to use ro-vibrational levels from the first excited state, $A^1\Sigma_u^+$, of the $Li_2$ dimer in the experiment. In particular, the molecules are prepared in the $A^1\Sigma_u^+(v = 5, J = 1)$ and $M = 0$ sublevel by excitation from the $X^1\Sigma_u^+(v = 0, J = 0)$ ground state level with linearly polarized light (the polarization direction is chosen to be the quantization axis). The other two sublevels, $M = \pm 1$, of the $A^1\Sigma_u^+(v = 5, J = 1)$ level are initially unpopulated. Here, the $M$ components are the projections of $\vec{J}$ on the axis defined by the polarization of the pump laser. The kinetics of the following process are studied:

$$\mathrm{Li_2}[A^1\Sigma_u^+(v = 5, J = 1, M = 0)] + NG \rightarrow \mathrm{Li_2}[A^1\Sigma_u^+(v = 5, J = 1, M \pm 1)] + NG, \quad (1)$$

where $NG$ represents a noble gas (either helium or argon) atom. In addition, we have studied the kinetics of $J$-changing inelastic collisions that transfer the molecules from the initial $A^1\Sigma_u^+(v = 5, J = 1)$ level to the neighboring $J = 3$, 5, and 7 rotational levels,

$$\mathrm{Li_2}[A^1\Sigma_u^+(v = 5, J = 1)] + NG \rightarrow \mathrm{Li_2}[A^1\Sigma_u^+(v = 5, J = 3, 5, 7)] + NG. \quad (2)$$

## II. THE EXPERIMENT

The experimental setup is shown in Fig. 1. The $Li_2$ molecules were created in a heatpipe oven[55] by evaporating lithium metal. The temperature of the oven was 780 K, determined from the Doppler FWHM of the $A^1\Sigma_u^+(v = 5, J = 1) \leftarrow X^1\Sigma_g^+(v = 0, J = 0)$ excitation line profile.[56] At this temperature, the lithium atomic and molecular vapor pressures are 4.05 mTorr and $2.85 \times 10^{-2}$ mTorr, respectively.[57] The desired pressure of the helium or argon gas was achieved by reducing the initial excess pressure of the buffer gas to the desired level. This procedure was carried out at the working temperature (780 K) of the oven. Thus, the measured pressure is a combination of the pressure of the lithium vapor and the noble atom buffer gas. The pressure was measured using a Baratron pressure transducer (MKS 626B12TBE) connected with quarter-inch tubing to the heatpipe oven. The same vacuum manifold, in combination with a set of Swagelok valves, was used to introduce and pump out the excess noble gas. The initial and final pressure measurements for each trial were typically within 0.01 Torr of each other. In the excitation scheme, a pair of counter-propagating dye lasers was used as the pump (Coherent 699-29, DCM dye) and probe (Coherent 699-29, R6G dye) lasers (designated $L1$ and $L2$, respectively; see Fig. 1). The laser bandwidths are each ~1 MHz. The spot size for each laser was ~1 mm in diameter in the interaction region.

Figure 2 shows schematically the energy levels and the $Li_2$ molecular states utilized in this study, including the relevant pump- and probe-laser excitation steps, and observed fluorescence channels. Specifics of the different $M$-changing collisional measurements are given in Figs. 3–5. The pump laser was tuned to the

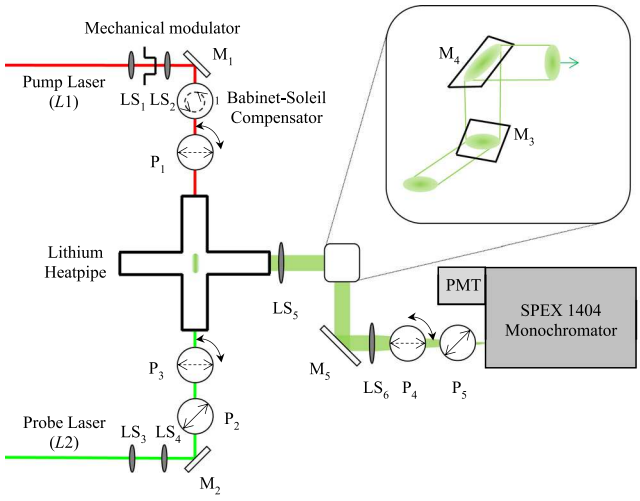


**FIG. 1**. Schematic depiction of the experimental setup. The pump (*L*1) and probe (*L*2) lasers (Coherent, Inc. model 699-29), operating with DCM and R6G dyes, respectively, are overlapped in the center of the heatpipe oven loaded with lithium metal. Laser induced fluorescence is collected at right angles to the laser propagation axis and directed to the entrance slits of the SPEX model 1404 monochromator.

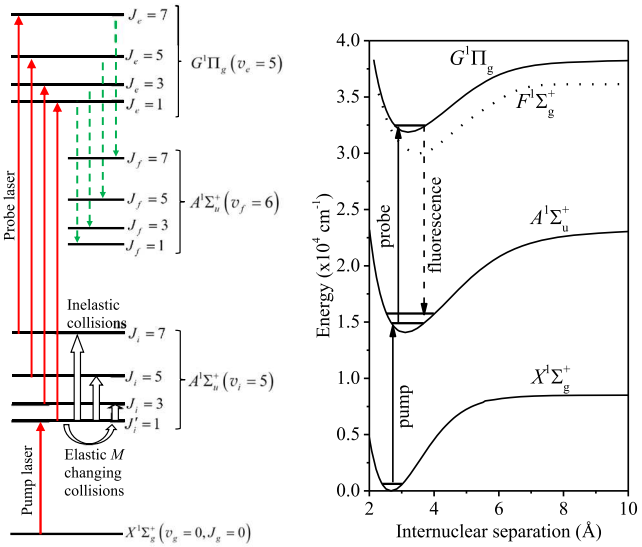


**FIG. 2**. The pump laser (15 251.98 $cm^{-1}$) excites the molecules from the $X^1\Sigma_g^+(v_g = 0, J_g = 0)$ rovibrational level of the ground electronic state to the $A^1\Sigma_u^+(v_i = 5, J_i = 1)$ rovibrational level of the first excited singlet electronic state. Elastic *M*-changing collisions taking place in the $A^1\Sigma_u^+(v_i = 5, J_i = 1)$ level are probed by Q-line excitation (17 654.50 $cm^{-1}$) to $G^1\Pi_g(v_e = 5, J_e = 1)$ and by P-line excitation (17 081.40 $cm^{-1}$) to $F^1\Sigma_g^+(v_e = 12, J_e = 0)$ (not shown in the figure). Fluorescence corresponding to transitions from the $G^1\Pi_g(v_e = 5, J_e = 1)$ and $F^1\Sigma_g^+(v_e = 12, J_e = 0)$ levels down to the $A^1\Sigma_u^+(v_f = 6, J_f = 1)$ level was detected at 574.13 nm and 593.66 nm, respectively. Inelastic *J*-changing collisions which populate the $A^1\Sigma_u^+(v_i = 5, J_i = 3, 5, 7)$ levels are probed by Q-line excitations to $G^1\Pi_g(v_e = 5, J_e = 3, 5, 7)$ at 17 654.22 $cm^{-1}$, 17 653.71 $cm^{-1}$, and 17 652.97 $cm^{-1}$, respectively. Fluorescence from the $G^1\Pi_g(v_e = 5, J_e = 3, 5, 7)$ levels is detected also as Q-branches terminating on the $A^1\Sigma_u^+(v_f = 6)$ vibrational manifold. The fluorescence transitions, Q(1) at 574.13 nm, Q(3) at 574.14 nm, Q(5) at 574.15 nm, and Q(7) at 574.17 nm, are all very closely spaced and within the transmission bandwidth (~0.75 nm) of the monochromator. Thus, for all measurements involving the $G^1\Pi_g$ state, the monochromator was set to 574.13 nm.

$Li_2$ $A^1\Sigma_u^+(v_i = 5, J_i = 1) \leftarrow X^1\Sigma_g^+(v_g = 0, J_g = 0)$ transition frequency in all measurements. The mixture of lithium vapor and noble gas is in thermal equilibrium in the heatpipe oven. Thus, the rotational state populations of the $Li_2$ molecules in the ground $X^1\Sigma_g^+$ electronic state follow the Boltzmann distribution, $N_J \propto (2J + 1)\exp[-B_v J(J + 1)/kT]$. The initial ground state rotational level $X^1\Sigma_g^+(v_g = 0, J_g = 0)$ is only weakly populated due to the small value of its degeneracy factor. Specifically, the population in the $J = 0$ level is ~4% of that in the most populated level, $J = 20$, at 780 K. Nevertheless, this population is sufficient for our purposes.

The pump laser beam was linearly polarized, with its polarization axis defining the quantization axis $\hat{\varepsilon}_{L1} \equiv \hat{k}$. Hence, the pump laser populated only the $M_i = 0$ magnetic sublevel of $A^1\Sigma_u^+(v_i = 5, J_i = 1)$. The probe laser was used to monitor the population in the directly excited level $A^1\Sigma_u^+(v_i = 5, J_i = 1, M_i = 0)$, as well as in the levels $A^1\Sigma_u^+(v_i = 5, J_i = 1, M_i = \pm 1)$, which were populated through elastic *M*-changing collisions (see Figs. 3–5), and the $A^1\Sigma_u^+(v_i = 5, J_i = 3)$, $A^1\Sigma_u^+(v_i = 5, J_i = 5)$, and $A^1\Sigma_u^+(v_i = 5, J_i = 7)$ levels that were populated through inelastic *J*-changing collisions (see Fig. 2), by inducing transitions to a higher lying level, $G^1\Pi_g(v_e = 5, J_e = J_i)$ or $F^1\Sigma_g^+(v_e = 12, J_e = J_i - 1)$. Here, we use subscripts *g*, *i*, *e*, and *f* on the *v*, *J* labels to indicate "ground," "intermediate," "excited," and "final" levels, respectively (see Figs. 3–5 and Sec. III A). The fluorescence emission from the excited state level *e* is partially polarized with its degree of polarization strongly dependent on the relative polarization of the lasers. Measurements were carried out with the four [horizontal–horizontal (HH), horizontal–vertical (HV), vertical–horizontal (VH), and vertical–vertical (VV)] possible polarization orientations of the pump and probe lasers, respectively.

The pump laser output was 99.7% linearly polarized in the vertical direction. To allow switching between horizontal and vertical polarizations without measurable asymmetry in their intensities, the linearly polarized output of the laser was first converted to circular polarization using a Babinet Soleil compensator (Karl Lambrecht Corp K1148). From the circularly polarized beam, either the horizontally or the vertically polarized component was selected using a polarizer, P1 (Glan Thompson). The linear polarization of the resulting beam was greater than 99.99%. The vertical or horizontal polarization orientation of the pump laser always served as the reference polarization axis (quantization axis) in these experiments. The output of the probe laser was also linearly polarized in the vertical direction. Switching between the horizontal and vertical orientations for this laser was achieved using a combination of two polarizers, P2 and P3. P2 rotated the polarization by 45° from the vertical (with 50% intensity loss) and P3 was set to transmit either the vertical or the horizontal component (with another 50% intensity loss). The angles

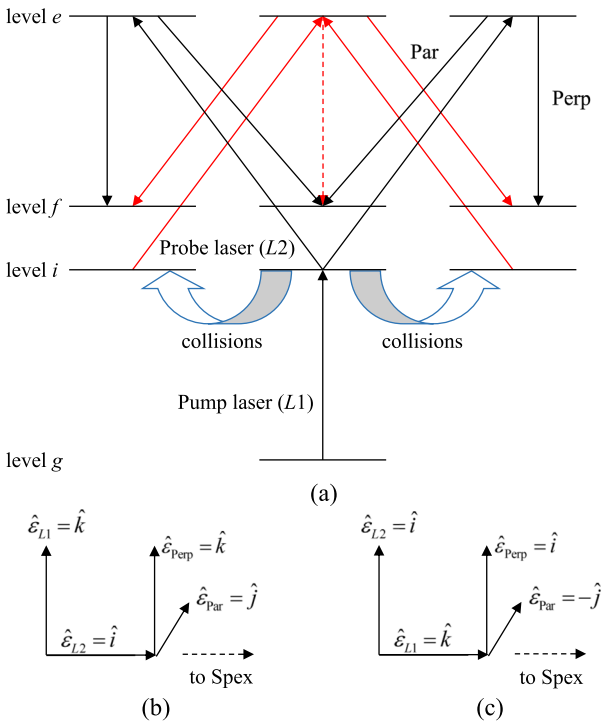


**FIG. 3**. (a) Pump/probe excitation scheme used to study *M*-changing collisions with the $G^1\Pi_g(v_e=5,J_e=J_i=1) \leftarrow A^1\Sigma_u^+(v_i=5,J_i=1)$ probe transition. Levels *g*, *i*, *e*, and *f* are the $Li_2$ $X^1\Sigma_g^+(v_g=0,J_g=0)$, $A^1\Sigma_u^+(v_i=5,J_i=1)$, $G^1\Pi_g(v_e=5,J_e=1)$, and $A^1\Sigma_u^+(v_f=6,J_f=1)$ levels, respectively. The pump laser polarization direction defines the quantization axis $(\hat{k})$, and in this case, the probe laser polarization was chosen to be perpendicular to the pump polarization direction. Probe laser excitation of molecules populating the directly excited magnetic sublevel $A^1\Sigma_u^+(v_i=5,J_i=1,M_i=0)$ and subsequent fluorescence channels $[G^1\Pi_g(v_e=5,J_e=J_i)\rightarrow A^1\Sigma_u^+(v_f=6,J_f=J_e)]$ are shown in black. Probe laser excitation of molecules in the collisionally populated magnetic sublevels $A^1\Sigma_u^+(v_i=5,J_i=1,M_i=\pm1)$ and subsequent fluorescence channels are shown in red. A dashed arrow indicates a forbidden transition. (b) Pump laser (*L*1) polarization vertical and probe laser (*L*2) polarization horizontal. (c) Pump laser (*L*1) polarization horizontal and probe laser (*L*2) polarization vertical. In either case, vertically and horizontally polarized fluorescence channels are designated "Perp" and "Par," respectively, corresponding to the fluorescence polarization direction perpendicular to, or parallel to, the Spex monochromator grating grooves (after a 90° rotation caused by the periscope). "Perp" and "Par" labels for vertical and diagonal fluorescence transitions in part (a) correspond to the geometry of part (b).

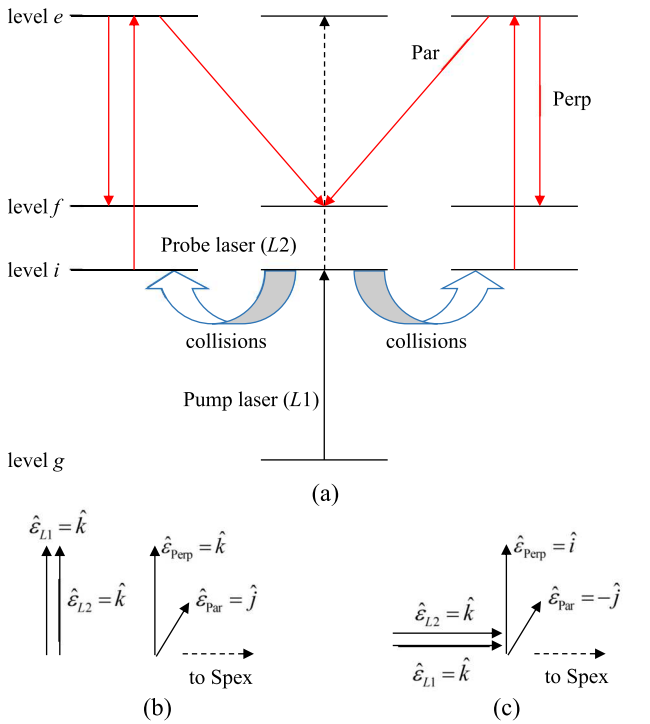


**FIG. 4**. (a) Pump/probe excitation scheme used to study *M*-changing collisions with the $G^1\Pi_g(v_e=5,J_e=J_i=1) \leftarrow A^1\Sigma_u^+(v_i=5,J_i=1)$ probe, as in Fig. 3, except that, here, the probe laser polarization was chosen to be parallel to the pump polarization direction. (b) Vertical pump (*L*1) and probe (*L*2) laser polarizations. (c) Horizontal pump (*L*1) and probe (*L*2) laser polarizations. "Perp" and "Par" labels for vertical and diagonal fluorescence transitions in part (a) correspond to the geometry of part (b).

for the vertical and horizontal polarization directions of P3 were set relative to the horizontal and vertical axes of P1 by finding the maximum and minimum transmission of the probe laser through P3 and P1. The orientation of the transmission axis of P2 was optimized for equal intensity for the horizontal and vertical transmissions of polarizer P3.

Florescence corresponding to a specific rovibrational channel was detected using a monochromator (SPEX 1404) as a narrow bandpass filter with its slits fully open at 3 mm width. The light transmitted through the monochromator was detected with a photomultiplier tube (PMT; Hamamatsu R928), which was cooled with a Peltier element and mounted at the exit slit. The experiments were performed by scanning the probe laser over the corresponding probe transition with the pump laser on resonance. The fluorescence signal from the PMT was amplified using a lock-in amplifier (Stanford Research Systems SR850 DSP) in conjunction with a mechanical chopper (Stanford Research Systems SR540), which modulated the pump laser beam intensity.

For the detection of fluorescence, the region where the laser beams overlapped was viewed through one of the side windows of the heatpipe. This horizontal cylinder in the center of the heatpipe was imaged onto the entrance slit of the monochromator using mirrors M3, M4, and M5 and lenses LS5 and LS6. Mirrors M3 and M4 form a 90° periscope, the purpose of which was to rotate the fluorescence image from horizontal to vertical to match the vertical orientation of the slits of the monochromator. The grooves of the two gratings (1800 g/mm) in the monochromator are also vertically oriented. The periscope also rotated the polarization of the detected fluorescence by 90°. Thus, the vertical and horizontal polarization components of the fluorescence emitted by molecules in the interaction region are perpendicular and parallel, respectively, to the grating groves at the entrance of the monochromator. For

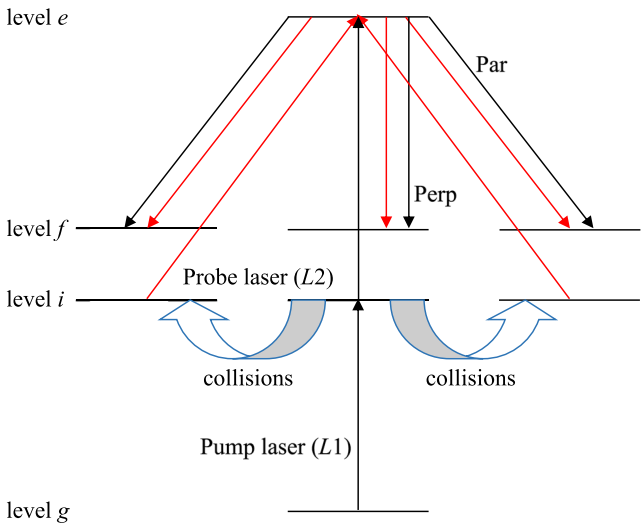


**FIG. 5**. Pump/probe excitation scheme used to study *M*-changing collisions with the $F^1\Sigma_g^+(v_e = 12, J_e = 0) \leftarrow A^1\Sigma_u^+(v_i = 5, J_i = 1)$ probe [in this case, levels *g*, *i*, and *f* are the same as in Figs. 3 and 4, but level *e* is the $F^1\Sigma_g^+(v_e = 12, J_e = 0)$ level]. The probe laser polarization was chosen to be either parallel or perpendicular to the pump polarization direction. With the probe laser polarization parallel to the pump polarization, the probe laser only excites molecules populating the directly excited magnetic sublevel, $A^1\Sigma_u^+(v_i = 5, J_i = 1, M_i = 0)$. This excitation channel and the subsequent fluorescence channels $\left[F^1\Sigma_g^+(v_e = 12, J_e = 0) \rightarrow A^1\Sigma_u^+(v_f = 6, J_f = 1)\right]$ are shown in black. With the probe laser polarization perpendicular to the pump polarization, the probe laser only excites molecules in the collisionally populated magnetic sublevels $A^1\Sigma_u^+(v_i = 5, J_i = 1, M_i = \pm 1)$. These excitation and subsequent fluorescence channels are shown in red. "Perp" and "Par" labels for vertical and diagonal fluorescence transitions in the figure correspond to the geometry of Figs. 3(b) and 4(b).

clarity, in the rest of this paper, the terms "horizontal" and "vertical" will be used exclusively to refer to the polarization axes of the lasers, and the symbols ∥ and ⊥ (indicating parallel and perpendicular, respectively) will refer to the relative orientations of the pump and probe laser polarizations. The fluorescence polarization components will be described using the terms "parallel" and "perpendicular" (denoted by subscripts "Par" and "Perp," respectively), indicating their orientation relative to the grating grooves. The polarizer P4 is used to selectively transmit either the perpendicular or the parallel polarization component of the fluorescence. The orientations of P4 for parallel and perpendicular transmission were determined using the following procedure. First, the spectrometer was set to 440 nm where the reflection efficiency of the gratings for light with perpendicular polarization is minimal.[58] The lasers were both blocked, and unpolarized white light from a tungsten-halogen lamp[59] was coupled to the system through the opposite side arm of the heatpipe. P4 was then rotated until the signal from the PMT at the exit slit of the monochromator was minimized, thus establishing the angle for P4 at which the perpendicular polarization component is transmitted. Then, the orientation of P4 for transmission of the parallel component was found by rotating P4 by ±90°. This was verified to be the case, with an accuracy of ±1°, by setting the monochromator to 655 nm (the minimal reflection efficiency of the gratings for polarization parallel to the groves of the gratings[58]) and rotating P4 until a minimal signal was observed. Polarizer P5 was installed between P4 and the entrance slit of the monochromator, with transmission axis oriented at 45° relative to the grooves of the gratings, in order to eliminate the difference in the monochromator's transmission efficiency for parallel and perpendicular polarizations. The precise orientation of the transmission axis of P5 was obtained as the half angle of the crossing angles of P5 with the parallel and perpendicular orientations of P4 while the heatpipe was illuminated with the unpolarized white light of the tungsten–halogen lamp.[59]

The spectrometer was then set to the detection wavelength, 574.13 nm [the center wavelength of the $G^1\Pi_g(v_e = 5, J_e = 1) \rightarrow A^1\Sigma_u^+(v_f = 6, J_f = 1)$ transition; see Figs. 2–5], for the experiment.

A second set of excitations was used to show that the collisionally induced transitions in the $(v_i = 5, J_i = 1)$ rotational level of the $A^1\Sigma_u^+$ electronic state were not dependent on the choice of the final electronic state. The $F(4)^1\Sigma_g^+$ electronic state was chosen for this as it lies in a similar energy region to the $G^1\Pi_g$ state, but has a different rotational character. The probe in this experiment transfers population from $A^1\Sigma_u^+(v_i = 5, J_i = 1)$ to $F(4)^1\Sigma_g^+(v_e = 12, J_e = 0)$ and fluorescence is detected on the $F(4)^1\Sigma_g^+(v_e = 12, J_e = 0) \rightarrow A^1\Sigma_u^+(v_f = 6, J_f = 1)$ transition at 593.66 nm. Finally, the collisionally induced changes in *J* of the intermediate state were measured by probing the $J_i = 3$, 5, or 7 Q-branch transitions $G^1\Pi_g(v_e = 5, J_e = J_i) \leftarrow A^1\Sigma_u^+(v_i = 5, J_i)$ and monitoring $G^1\Pi_g(v_e = 5, J_e) \rightarrow A^1\Sigma_u^+(v_f = 6, J_f = J_e)$ fluorescence (see Fig. 2).

Laser powers varied between 150 mW and 400 mW over the course of the experiments; however, the laser power did not vary by more than 10 mW over a single set of measurements. In most cases, the probe laser was scanned over 6 GHz with a step size of 2 MHz. Each step was averaged 150 times. Since the spectral lines are significantly pressure broadened above 10 Torr, the probe laser scans were a little broader (10 GHz long with 5 MHz steps) at these higher pressures to make sure there was sufficient data to allow a good baseline to be determined. Each scan was analyzed by first averaging and subtracting the baseline and then integrating the peak to determine the total emission from the transition. The total emissions for various combinations of laser and fluorescence polarizations were then combined as described in Sec. III to find the relative population that had transitioned from $M_i = 0$ to $M_i = \pm 1$ or from $J_i = 1$ to $J_i = 3$, 5, or 7 during a collision. The experimental range of pressures used was 0.3 Torr–30 Torr.

## III. ANALYSIS AND RESULTS

### A. Level densities in terms of measured fluorescence signals

We label the lower level of the pump transition, $X^1\Sigma_g^+(v_g = 0, J_g = 0)$, as level *g* (ground), the lower level of the probe transition [either $A^1\Sigma_u^+(v_i = 5, J_i = 1, M_i = 0)$ (the level directly excited by the pump), or $A^1\Sigma_u^+(v_i = 5, J_i = 1, M_i = \pm 1)$ (a particular collisionally populated *M* level), or $A^1\Sigma_u^+(v_i = 5, J_i = 3, 5, 7)$ (a neighboring collisionally populated *J* level)] as level *i* (intermediate), the upper level

of the probe transition [$G^1\Pi_g(v_e = 5, J_e = J_i)$ or $F^1\Sigma_g^+(v_e = 12, J_e = 0)$] as level $e$ (excited), and the lower level of the observed fluorescence channel [either $A^1\Sigma_u^+(v_f = 6, J_f = J_e)$ or $A^1\Sigma_u^+(v_f = 6, J_f = 1)$] as level $f$ (final).

According to Jones *et al.*[33] [Eq. (5)], the fluorescence intensity for a transition from excited (upper) level $|e\rangle$ to final (lower) level $|f\rangle$ is given by

$$I = h\nu_{e\to f} n_e V A_{e\to f} \varepsilon_{e\to f} \frac{d\Omega}{4\pi} F, \tag{3}$$

where $n_e$ is the density of molecules in level $|e\rangle$, $A_{e\to f}$ is the spontaneous emission rate (Einstein $A$ coefficient) for the transition from level $|e\rangle$ to level $|f\rangle$, $\varepsilon_{e\to f}$ is the detection system efficiency at frequency $\nu_{e\to f}$, $V$ is the detection volume within the heatpipe, $d\Omega$ is the detection solid angle, and $F$ is a geometric factor that takes into account the fact that oscillating dipoles do not radiate isotropically. Specifically, an oscillating dipole moment oriented along a particular direction $\hat{e}$ will emit fluorescence polarized along $\hat{e}$ with maximum intensity in directions perpendicular to $\hat{e}$ and zero intensity in the direction along $\hat{e}$. Any dipole moment can be decomposed into components along the three coordinate directions, $\hat{i}$, $\hat{j}$, and $\hat{k}$. Therefore, we could dispense with the factor $F$ if we could ensure that we were equally sensitive to all dipole components (i.e., if the measured intensity signal was defined to be $I \equiv I_{\hat{i}} + I_{\hat{j}} + I_{\hat{k}}$). As can be seen in Fig. 3(b) (where the pump laser polarization defines $\hat{k}$ as vertical), the vertically polarized fluorescence signal (with the polarization vector labeled $\hat{\varepsilon}_{\mathrm{Perp}}$) is maximally sensitive to dipole components oriented along $\hat{k}$, while the horizontally polarized fluorescence signal (with the polarization vector labeled $\hat{\varepsilon}_{\mathrm{Par}}$) is maximally sensitive to dipole components oriented along $\hat{j}$ (i.e., $I_{\mathrm{Perp}} = I_{\hat{k}}$ and $I_{\mathrm{Par}} = I_{\hat{j}}$). With this configuration of lasers and detection system, it is not possible to observe fluorescence from dipole components oriented along $\hat{i}$, and it is inconvenient to move the detection system. However, we can achieve the same thing, while in this example maintaining the pump and probe laser polarization directions perpendicular to each other, by orienting the pump laser polarization in the horizontal direction and the probe laser polarization in the vertical direction [see Fig. 3(c)]. In this latter case, the pump laser polarization still defines the quantization axis $\hat{k}$, the probe laser polarization still defines the $\hat{i}$ direction, and $I_{\mathrm{Perp}} = I_{\hat{i}}$. Thus, we can rewrite Eq. (3) as

$$I \equiv I_{\mathrm{Perp}}^{VH} + I_{\mathrm{Par}}^{VH} + I_{\mathrm{Perp}}^{HV} = h\nu_{e\to f} n_e V A_{e\to f} \varepsilon_{e\to f} \frac{d\Omega}{4\pi}, \tag{4}$$

where the first and second superscripts indicate the pump and probe laser polarization directions, respectively, (i.e., $I_{\mathrm{Perp}}^{VH}$ indicates the observed fluorescence signal, with polarization perpendicular to the monochromator grating grooves, recorded with pump laser polarization vertical and probe laser polarization horizontal). We also note that, in principle, $I_{\mathrm{Par}}^{HV} = I_{\mathrm{Par}}^{VH}$ and thus contains no new information.

The same analysis of the fluorescence signals remains valid if the probe laser polarization is parallel to the pump laser polarization. Therefore, we can now define

$$I^{\perp} \equiv I_{\mathrm{Perp}}^{VH} + I_{\mathrm{Par}}^{VH} + I_{\mathrm{Perp}}^{HV} \tag{5}$$

and

$$I^{\parallel} \equiv I_{\mathrm{Perp}}^{VV} + I_{\mathrm{Par}}^{VV} + I_{\mathrm{Perp}}^{HH}, \tag{6}$$

where the superscript now indicates whether the laser polarizations are perpendicular or parallel to each other. Note that these two intensity signals, with each being a sum of three measured intensities, are directly proportional to the total population in the upper level and are independent of any subsequent collisional redistribution of population among the upper state $M$ sublevels.

Next, we must relate the upper level densities to the intermediate level densities that we probe.

### 1. M-changing collisions—Probe $G^1\Pi_g(v_e = 5, J_e = 1) \leftarrow A^1\Sigma_u^+(v_i = 5, J_i = 1)$

To study $M_i = 0 \to M_i = \pm 1$ ($M$-changing) collisions of noble gas perturbers with $Li_2$ molecules in the $A^1\Sigma_u^+(v = 5, J = 1)$ state, using the $G^1\Pi_g(v_e = 5, J_e = 1) \leftarrow A^1\Sigma_u^+(v_i = 5, J_i = 1)$ probe transition, we make six separate measurements ($I_{\mathrm{Perp}}^{VH}$, $I_{\mathrm{Par}}^{VH}$, $I_{\mathrm{Perp}}^{HV}$, $I_{\mathrm{Perp}}^{VV}$, $I_{\mathrm{Par}}^{VV}$, $I_{\mathrm{Perp}}^{HH}$) and form the combinations $I^{\perp} = I_{\mathrm{Perp}}^{VH} + I_{\mathrm{Par}}^{VH} + I_{\mathrm{Perp}}^{HV}$ and $I^{\parallel} = I_{\mathrm{Perp}}^{VV} + I_{\mathrm{Par}}^{VV} + I_{\mathrm{Perp}}^{HH}$ as described above. As shown in Appendix A of the supplementary material, the upper level population is given by

$$n_e \propto n_i e^2 |E_{L2}\hat{\varepsilon}_{L2} \cdot \langle \alpha_e, v_e, J_e, M_e|\vec{r}|\alpha_i, v_i, J_i, M_i\rangle|^2, \tag{7}$$

where $E_{L2}$ and $\hat{\varepsilon}_{L2}$ are the electric field amplitude and polarization vector of the probe laser, and $-e\langle \alpha_e, v_e, J_e, M_e|\vec{r}|\alpha_i, v_i, J_i, M_i\rangle$ is the electric dipole matrix element of the transition. For $\Delta J = 0$, the $M = 0 \to M = 0$ probe transition is forbidden, so that when the probe laser polarization is parallel to the pump laser polarization (i.e., when the probe polarization is along the quantization axis), we only excite molecules in the collisionally populated intermediate levels $A^1\Sigma_u^+(v_i = 5, J_i = 1, M_i = \pm 1)$ [vertical probe transitions in Fig. 4(a)]. When the probe laser polarization is perpendicular to the pump laser polarization [Fig. 3(a)], we excite molecules in the directly excited level $A^1\Sigma_u^+(v_i = 5, J_i = 1, M_i = 0)$ as well as those in the collisionally populated levels $A^1\Sigma_u^+(v_i = 5, J_i = 1, M_i = \pm 1)$. Specifically, it is straightforward to show (see Appendix A of the supplementary material) that

$$I^{\perp} \propto \frac{(n_{J_i=1,M_i=-1} + 2n_{J_i=1,M_i=0} + n_{J_i=1,M_i=+1})}{2} \times e^2 (E_{L2})^2 |(\alpha_e, v_e, J_e = 1|\vec{r}|\alpha_i, v_i, J_i = 1)|^2 \tag{8}$$

and

$$I^{\parallel} \propto (n_{J_i=1,M_i=-1} + n_{J_i=1,M_i=+1}) \times e^2 (E_{L2})^2 |(\alpha_e, v_e, J_e = 1|\vec{r}|\alpha_i, v_i, J_i = 1)|^2, \tag{9}$$

where $n_{J_i,M_i}$ represents the density or population of molecules in level $J_i$, $M_i$, and $(\alpha_e, v_e, J_e = 1|\vec{r}|\alpha_i, v_i, J_i = 1)$ is the reduced matrix element of Condon and Shortley.[60] The proportionality factors are the

same (see Appendix A of the supplementary material) so that the combination

$$\left[\frac{2I^{\parallel}}{2I^{\perp}-I^{\parallel}}\right]_{\text{Probe } J_i=1\rightarrow G^1\Pi_g} = \frac{\left(n_{J_i=1,M_i=-1}+n_{J_i=1,M_i=+1}\right)}{n_{J_i=1,M_i=0}} \tag{10}$$

is a measure of the ratio of population in the collisionally populated levels $A^1\Sigma_u^+(v_i=5, J_i=1, M_i=\pm1)$ to that in the directly populated level $A^1\Sigma_u^+(v_i=5, J_i=1, M_i=0)$. By symmetry, $n_{J_i=1,M_i=-1} = n_{J_i=1,M_i=+1}$, so we can also write

$$R_{J_i=1(G^1\Pi_g)} \equiv \left[\frac{I^{\parallel}}{2I^{\perp}-I^{\parallel}}\right]_{\text{Probe } J_i=1\rightarrow G^1\Pi_g} = \frac{n_{J_i=1,M_i=\pm1}}{n_{J_i=1,M_i=0}}, \tag{11}$$

where $n_{J_i=1,M_i=\pm1}$ represents the population in either the $M_i=-1$ or the $M_i=+1$ sublevel (not the sum).

### 2. M-changing collisions–Probe $F^1\Sigma_g^+$ ($v_e$ = 12,$J_e$ = 0) ← $A^1\Sigma_u^+$ ($v_i$ = 5,$J_i$ = 1)

As a check, we also studied $M_i = 0 \rightarrow M_i = \pm1$ transfer of population in collisions of argon atoms with $Li_2$ molecules in the $A^1\Sigma_u^+(v_i=5, J_i=1)$ level using the $F^1\Sigma_g^+(v_e=12, J_e=0) \leftarrow A^1\Sigma_u^+(v_i=5, J_i=1)$ probe transition. In this case, the rotational level of the upper state of the transition is $J_e=0$, with only one magnetic sublevel $M_e=0$. Consequently, when the probe laser polarization is parallel to the pump laser polarization, we only probe $A^1\Sigma_u^+(v_i=5, J_i=1, M_i=0)$, and when the probe laser polarization is perpendicular to the pump laser polarization, we only probe $A^1\Sigma_u^+(v_i=5, J_i=1, M_i=\pm1)$ (see Fig. 5).

In this case, the analysis is relatively simple, and it is straightforward to show [see Appendix A of the supplementary material, Eq. (A25)] that

$$R_{J_i=1(F^1\Sigma_g^+)} \equiv \left[\frac{I^{\perp}}{I^{\parallel}}\right]_{\text{Probe } J_i=1\rightarrow F^1\Sigma_g^+} = \frac{n_{v_i,J_i=1,M_i=\pm1}}{n_{v_i,J_i=1,M_i=0}}. \tag{12}$$

Although use of this probe transition yields a much simpler and cleaner interpretation of the data, we discovered that these signals were all very much smaller than those obtained using the $G^1\Pi_g(v_e=5, J_e=J_i=1) \leftarrow A^1\Sigma_u^+(v_i=5, J_i=1)$ probe transitions. This led to much larger uncertainties in the ratios of collisionally populated to directly populated $M$ levels. For this reason, we recorded a very limited number of measurements using the $F^1\Sigma_g^+(v_e=12, J_e=0) \leftarrow A^1\Sigma_u^+(v_i=5, J_i=1)$ probe transition, and concentrated our efforts on those obtained using $G^1\Pi_g \leftarrow A^1\Sigma_u^+$ probe transitions. Nonetheless, all of the measurements obtained using both probe transitions were used in the fits with appropriate weighting.

### 3. J-changing collisions–Probe $G^1\Pi_g$($v_e$ = 5,$J_e$ = $J_i$) ← $A^1\Sigma_u^+$ ($v_i$ = 5,$J_i$ = 3,5,7) and $G^1\Pi_g$($v_e$ = 5,$J_e'$ = $J_i'$) ← $A^1\Sigma_u^+$ ($v_i$ = 5,$J_i'$ = 1)

For our $J$-changing collision experiments, we again make six separate measurements ($I_{\text{Perp}}^{VH}$, $I_{\text{Par}}^{VH}$, $I_{\text{Perp}}^{HV}$, $I_{\text{Perp}}^{VV}$, $I_{\text{Par}}^{VV}$, $I_{\text{Perp}}^{HH}$) for each of the collisionally populated rotational levels under study ($J_i$ = 3, 5, and 7) of $A^1\Sigma_u^+(v_i=5)$ and for the directly excited level $A^1\Sigma_u^+(v_i=5, J_i'=1)$ (including $M_i'=0$ and $M_i'=\pm1$). Here, we use primes to indicate the rotational quantum numbers of the directly excited intermediate level $A^1\Sigma_u^+(v_i=5, J_i'=1)$ [and of the upper excited level $G^1\Pi_g(v_e=5, J_e'=J_i')$ coupled to this level by the probe laser]. We then evaluate the combinations $I^{\perp} \equiv I_{\text{Perp}}^{VH} + I_{\text{Par}}^{VH} + I_{\text{Perp}}^{HV}$ and $I^{\parallel} \equiv I_{\text{Perp}}^{VV} + I_{\text{Par}}^{VV} + I_{\text{Perp}}^{HH}$ for each of these levels. As demonstrated in Appendix A of the supplementary material, the ratio of density of a particular collisionally populated level to the density of the directly excited level, is related to these measured intensities by

$$R_{J_i=3,5,7} \equiv \frac{\left[2I^{\perp}+I^{\parallel}\right]_{\text{Probe } J_i=3,5,7\rightarrow G^1\Pi_g}}{\left[2I^{\perp}+I^{\parallel}\right]_{\text{Probe } J_i'=1\rightarrow G^1\Pi_g}} = \frac{\sum_{M_i=-J_i}^{J_i} n_{J_i=3,5,7,M_i}}{\sum_{M_i'=-J_i'}^{J_i'} n_{J_i'=1,M_i'}} = \frac{n_{J_i=3,5,7}}{n_{J_i'=1}}. \tag{13}$$

It should be noted that in the analysis presented above, we have neglected the potentially depolarizing effects of hyperfine structure and stray electric and magnetic fields. The largest contributor to hyperfine structure of rotational levels of alkali diatomic molecules is the $\vec{I}\cdot\vec{S}$ Fermi contact interaction, which is absent in the spin singlet states of interest here. Other contributors to the hyperfine structure of $Li_2$ singlet states are expected to be very much smaller than the laser bandwidth and homogenous linewidth and are not resolvable under our experimental conditions. Also, since $Li_2$ is homonuclear (has inversion symmetry and hence no permanent electric dipole moment), and for a $^1\Sigma$ state the quantum numbers $\Lambda$ and S are both zero, we expect that first order Stark and Zeeman effects are zero. Therefore, any Stark and Zeeman splittings of the $Li_2$ $A^1\Sigma_u^+$ state, due to stray electric and magnetic fields (including the earth's magnetic field), are calculated to be much smaller than the laser bandwidth or homogeneous linewidth and can thus be neglected.

## B. Rate equations

### 1. M-changing collisions

The levels $A^1\Sigma_u^+(v_i=5, J_i=1, M_i=\pm1)$ are populated by $M$-changing collisions and are depopulated by quenching collisions, spontaneous emission, and probe laser excitation. Thus, we can write a steady-state rate equation for the densities in these levels as

$$\begin{aligned}\dot{n}_{J_i=1,M_i=\pm1} &= 0 \\ &= \left[k_{NG}^{J_i=1,M_i=0\rightarrow\pm1} n_{NG} + k_{Li}^{J_i=1,M_i=0\rightarrow\pm1} n_{Li}\right] n_{J_i=1,M_i=0} \\ &\quad + P_{\text{Probe}}^{e\rightarrow J_i=1,M_i=\pm1} n_e - \left[\Gamma_{J_i=1} + k_{NG}^{Q,J_i=1,M_i=\pm1} n_{NG}\right. \\ &\quad \left. + k_{Li}^{Q,J_i=1,M_i=\pm1} n_{Li} + P_{\text{Probe}}^{e\leftarrow J_i=1,M_i=\pm1}\right] n_{J_i=1,M_i=\pm1}. \end{aligned} \tag{14}$$

In this expression, $k_{NG}^{J_i=1,M_i=0\rightarrow\pm1}$ and $k_{Li}^{J_i=1,M_i=0\rightarrow\pm1}$ are the rate coefficients for collisions that cause $M_i=0 \rightarrow M_i=\pm1$ population transfer with noble gas and lithium atom perturbers, respectively, $k_{NG}^{Q,J_i=1,M_i=\pm1}$ and $k_{Li}^{Q,J_i=1,M_i=\pm1}$ are the rate coefficients for $J_i=1$, $M_i=\pm1$ quenching collisions (any collisions that depopulate

$J_i = 1$, $M_i = \pm 1$ regardless of the final state) with noble gas or lithium atom perturbers, $\Gamma_{J_i=1}$ is the total radiative rate out of level $J_i = 1$ (note: the total spontaneous emission rate is identical for all $M_i$ sublevels), and $P^{e\leftarrow J_i=1,M_i=\pm1}_{\text{Probe}}$ and $P^{e\rightarrow J_i=1,M_i=\pm1}_{\text{Probe}}$ are the rates for absorption and stimulated emission induced by the probe laser. $n_{NG}$ and $n_{Li}$ are the densities of noble gas and lithium atom collision partners. In Eq. (14), we have neglected multiple collision processes (but see below). Solving for the ratio $n_{J_i=1,M_i=\pm1}/n_{J_i=1,M_i=0}$, we find

$$\frac{n_{J_i=1,M_i=\pm1}}{n_{J_i=1,M_i=0}} = \frac{k_{NG}^{J_i=1,M_i=0\rightarrow\pm1} n_{NG} + k_{Li}^{J_i=1,M_i=0\rightarrow\pm1} n_{Li}}{\Gamma_{J_i=1} + k_{NG}^{Q,J_i=1,M_i=\pm1} n_{NG} + k_{Li}^{Q,J_i=1,M_i=\pm1} n_{Li} + P^{e\leftarrow J_i=1,M_i=\pm1}_{\text{Probe}} - P^{e\rightarrow J_i=1,M_i=\pm1}_{\text{Probe}} \frac{n_e}{n_{J_i=1,M_i=\pm1}}}. \tag{15}$$

In the weak probe field limit, we may neglect the probe laser excitation and stimulated emission terms (the last two terms in the denominator). Therefore, the ratio of density in a collisionally populated level ($J_i = 1$, $M_i = \pm1$) to the density in the level directly populated by the pump laser ($J_i = 1$, $M_i = 0$) is given by

$$\frac{n_{J_i=1,M_i=\pm1}}{n_{J_i=1,M_i=0}} = \frac{k_{NG}^{J_i=1,M_i=0\rightarrow\pm1} n_{NG} + k_{Li}^{J_i=1,M_i=0\rightarrow\pm1} n_{Li}}{\Gamma_{J_i=1} + k_{NG}^{Q,J_i=1,M_i=\pm1} n_{NG} + k_{Li}^{Q,J_i=1,M_i=\pm1} n_{Li}}. \tag{16}$$

[We also note that in the strong probe field limit, the last two terms in the denominator of Eq. (15) will cancel, and so Eq. (16) is also valid in that limit.]

### 2. J-changing collisions

The situation is similar for $J$-changing collisions, except that in this case, we eventually incorporate the effects of multiple collision processes. The steady-state rate equation for the density in a particular level ($J_i = 3$, 5, or 7) populated by $J$-changing collisions is

$$\begin{aligned}\dot{n}_{J_i=3,5,7} &= 0 \\ &= \left[k_{NG}^{J_i'=1\rightarrow J_i=3,5,7} n_{NG} + k_{Li}^{J_i'=1\rightarrow J_i=3,5,7} n_{Li}\right] n_{J_i'=1} \\ &\quad + \sum_{J\neq1,J_i} \left\{\left[k_{NG}^{J\rightarrow J_i=3,5,7} n_{NG} + k_{Li}^{J\rightarrow J_i=3,5,7} n_{Li}\right] n_J\right\} + P^{e\rightarrow J_i=3,5,7}_{\text{Probe}} n_e \\ &\quad - \left[\Gamma_{J_i=3,5,7} + k_{NG}^{Q,J_i=3,5,7} n_{NG} + k_{Li}^{Q,J_i=3,5,7} n_{Li} + P^{e\leftarrow J_i=3,5,7}_{\text{Probe}}\right] n_{J_i=3,5,7}.\end{aligned} \tag{17}$$

Here, $k_{NG}^{J\rightarrow J_i=3,5,7}$ and $k_{Li}^{J\rightarrow J_i=3,5,7}$ are rate coefficients for transfer of population from level $J$ to level $J_i = 3$, 5, 7 in collisions ($J$-changing collisions) of $Li_2$ molecules in state $A^1\Sigma_u^+(v_i = 5, J)$ with noble gas and lithium atoms, respectively, and $k_{NG}^{Q,J_i=3,5,7}$ and $k_{Li}^{Q,J_i=3,5,7}$ are the corresponding quenching rate coefficients. In the weak probe laser limit, the solution to Eq. (17) is

$$\frac{n_{J_i=3,5,7}}{n_{J_i'=1}} = \frac{\left[k_{NG}^{J_i'=1\rightarrow J_i=3,5,7} n_{NG} + k_{Li}^{J_i'=1\rightarrow J_i=3,5,7} n_{Li}\right] + \sum_{J\neq1,J_i} \left[k_{NG}^{J\rightarrow J_i=3,5,7} n_{NG} + k_{Li}^{J\rightarrow J_i=3,5,7} n_{Li}\right] \frac{n_J}{n_{J_i'=1}}}{\Gamma_{J_i=3,5,7} + k_{NG}^{Q,J_i=3,5,7} n_{NG} + k_{Li}^{Q,J_i=3,5,7} n_{Li}}. \tag{18}$$

[This equation is also valid in the strong probe field (saturation) limit since the absorption and stimulated emission terms also cancel in that case.]

## C. Fitting the data

### 1. Single collision approximation

Combining Eqs. (11) and (16), we obtain the following relationship between the measured intensities when probing the $G^1\Pi_g(v_e = 5, J_e = 1) \leftarrow A^1\Sigma_u^+(v_i = 5, J_i = 1)$ transition and the $M$-changing collision rate coefficients that we wish to determine:

$$R_{J_i=1(G^1\Pi_g)} = \left[\frac{I^{\parallel}}{2I^{\perp} - I^{\parallel}}\right]_{\text{Probe } J_i=1\rightarrow G^1\Pi_g} = \frac{k_{NG}^{J_i=1,M_i=0\rightarrow\pm1} n_{NG} + k_{Li}^{J_i=1,M_i=0\rightarrow\pm1} n_{Li}}{\Gamma_{J_i=1} + k_{NG}^{Q,J_i=1,M_i=\pm1} n_{NG} + k_{Li}^{Q,J_i=1,M_i=\pm1} n_{Li}}. \tag{19}$$

Similarly, we combine (12) and (16) to obtain the following relationship between the measured intensities when probing the $F^1\Sigma_g^+(v_e = 12, J_e = 0) \leftarrow A^1\Sigma_u^+(v_i = 5, J_i = 1)$ transition and the $M$-changing collision rate coefficients:

$$R_{J_i=1(F^1\Sigma_g^+)} \equiv \left[\frac{I^\perp}{I^\parallel}\right]_{\text{Probe } J_i=1\rightarrow F^1\Sigma_g^+} = \frac{k_{NG}^{J_i=1,M_i=0\rightarrow\pm1} n_{NG} + k_{Li}^{J_i=1,M_i=0\rightarrow\pm1} n_{Li}}{\Gamma_{J_i=1} + k_{NG}^{Q,J_i=1,M_i=\pm1} n_{NG} + k_{Li}^{Q,J_i=1,M_i=\pm1} n_{Li}}. \tag{20}$$

And finally, we can combine Eqs. (13) and (18) to obtain the relationship between measured intensities when probing the $G^1\Pi_g(v_e = 5, J_e = J_i) \leftarrow A^1\Sigma_u^+(v_i = 5, J_i = 3, 5, 7)$ and $G^1\Pi_g\left(v_e = 5, J_e' = J_i'\right) \leftarrow A^1\Sigma_u^+\left(v_i = 5, J_i' = 1\right)$ transitions and the rate coefficients for $J$-changing collisions:

$$\begin{aligned} R_{J_i=3,5,7} &= \frac{\left[2I^\perp + I^\parallel\right]_{\text{Probe } J_i=3,5,7\rightarrow G^1\Pi_g}}{\left[2I^\perp + I^\parallel\right]_{\text{Probe } J_i'=1\rightarrow G^1\Pi_g}} \\ &= \frac{k_{NG}^{J_i'=1\rightarrow J_i=3,5,7} n_{NG} + k_{Li}^{J_i'=1\rightarrow J_i=3,5,7} n_{Li} + \sum_{J\neq1,J_i}\left[k_{NG}^{J\rightarrow J_i=3,5,7} n_{NG} + k_{Li}^{J\rightarrow J_i=3,5,7} n_{Li}\right]\frac{n_J}{n_{J_i'=1}}}{\Gamma_{J_i=3,5,7} + k_{NG}^{Q,J_i=3,5,7} n_{NG} + k_{Li}^{Q,J_i=3,5,7} n_{Li}}. \end{aligned} \tag{21}$$

Following Jones *et al.*,[33] we make the assumption that for a particular perturber (argon, helium, or lithium) the quenching rates are approximately equal for the four levels ($J_i$ = 1, 3, 5, and 7) under consideration in this work. This approximation is justified by the theoretical calculations of Price[46] (in particular, see Fig. 6 of Ref. 33 and the related discussion). In the current work, the oven temperature was maintained at an approximately constant value of 780 K. Consequently, the lithium density was also approximately constant ($\sim 5.0 \times 10^{13}$ cm$^{-3}$) and the $M$-changing, $J$-changing, and quenching terms due to lithium collisions can be replaced by constants in Eqs. (19)–(21). Also, as discussed in Appendix A, found in the supplementary material [see Eqs. (A32)–(A37) and subsequent text], we can set the total radiative rates equal for the four levels (i.e., $\Gamma_{J_i=1} = \Gamma_{J_i=3} = \Gamma_{J_i=5} = \Gamma_{J_i=7} \equiv \Gamma$). In addition, we express the rate coefficients in units of $\Gamma$ by introducing the notation $\tilde{k} = k/\Gamma$. Finally, in this initial round of fitting, we neglect multiple collision processes [i.e., the sum over $J$ in Eq. (21)]. Thus, we obtain

$$R_{J_i=1(G^1\Pi_g)} = \left[\frac{I^\parallel}{2I^\perp - I^\parallel}\right]_{\text{Probe } J_i=1\rightarrow G^1\Pi_g} = \frac{\tilde{k}_{NG}^{J_i=1,M_i=0\rightarrow\pm1} n_{NG} + C_1}{1 + \tilde{k}_{NG}^{Q} n_{NG} + C_Q}, \tag{22}$$

$$R_{J_i=1(F^1\Sigma_g^+)} = \left[\frac{I^\perp}{I^\parallel}\right]_{\text{Probe } J_i=1\rightarrow F^1\Sigma_g^+} = \frac{\tilde{k}_{NG}^{J_i=1,M_i=0\rightarrow\pm1} n_{NG} + C_1}{1 + \tilde{k}_{NG}^{Q} n_{NG} + C_Q}, \tag{23}$$

and

$$R_{J_i=3,5,7} = \frac{\left[2I^\perp + I^\parallel\right]_{\text{Probe } J_i=3,5,7\rightarrow G^1\Pi_g}}{\left[2I^\perp + I^\parallel\right]_{\text{Probe } J_i'=1\rightarrow G^1\Pi_g}} = \frac{\left[\tilde{k}_{NG}^{J_i'=1\rightarrow J_i=3,5,7} n_{NG} + C_{3,5,7}\right]}{1 + \tilde{k}_{NG}^{Q} n_{NG} + C_Q}, \tag{24}$$

for the $M$-changing data obtained using the $G^1\Pi_g(v_e = 5, J_e = 1) \leftarrow A^1\Sigma_u^+(v_i = 5, J_i = 1)$ probe transition, $M$-changing data obtained using the $F^1\Sigma_g^+(v_e = 12, J_e = 0) \leftarrow A^1\Sigma_u^+(v_i = 5, J_i = 1)$ probe transition, and $J$-changing data obtained using the $G^1\Pi_g(v_e = 5, J_e = J_i) \leftarrow A^1\Sigma_u^+(v_i = 5, J_i = 3, 5, 7)$ and $G^1\Pi_g\left(v_e = 5, J_e' = J_i'\right) \leftarrow A^1\Sigma_u^+\left(v_i = 5, J_i' = 1\right)$ probe transitions, respectively. $M$-changing collision and $J$-changing collision data collected using either argon or helium as a buffer gas were fit simultaneously, using the nonlinear multiple regression tool of Origin version 9.3 (2016). For each data point, the independent variables are the noble gas type (either argon or helium), the noble gas density, and the relevant $J_i$ level, while the dependent variable is the left hand side of Eqs. (22), (23) or (24) obtained from the measured fluorescence intensities. The fitting parameters are the ten rate coefficients in units of the decay rate $\Gamma$ (i.e.; $\tilde{k}_{Ar}^{J_i=1,M_i=0\rightarrow\pm1}$, $\tilde{k}_{He}^{J_i=1,M_i=0\rightarrow\pm1}$, $\tilde{k}_{Ar}^{J_i'=1\rightarrow J_i=3}$, $\tilde{k}_{He}^{J_i'=1\rightarrow J_i=3}$, $\tilde{k}_{Ar}^{J_i'=1\rightarrow J_i=5}$, $\tilde{k}_{He}^{J_i'=1\rightarrow J_i=5}$, $\tilde{k}_{Ar}^{J_i'=1\rightarrow J_i=7}$, $\tilde{k}_{He}^{J_i'=1\rightarrow J_i=7}$, $\tilde{k}_{Ar}^{Q}$ and $\tilde{k}_{He}^{Q}$) and the five lithium parameters ($C_1$, $C_3$, $C_5$, $C_7$, and $C_Q$). As we will see, the lithium contributions are all extremely small, and ultimately the lithium terms were all set to zero in our fits.

Error bars for each data point depend on the uncertainties in the measured intensities and uncertainty in the noble gas density. Our version of Origin does not allow nonlinear multiple regression fitting with errors in both dependent and independent variables. Thus, we incorporated the uncertainty in the noble gas density into the uncertainty in the dependent variable using

$$\Delta R_{J_i} = \left|\frac{dR_{J_i}}{dI_{\text{Perp}}^{VH}}\right|\Delta I_{\text{Perp}}^{VH} + \left|\frac{dR_{J_i}}{dI_{\text{Par}}^{VH}}\right|\Delta I_{\text{Par}}^{VH} + \left|\frac{dR_{J_i}}{dI_{\text{Perp}}^{HV}}\right|\Delta I_{\text{Perp}}^{HV} + \left|\frac{dR_{J_i}}{dI_{\text{Perp}}^{VV}}\right|\Delta I_{\text{Perp}}^{VV} + \left|\frac{dR_{J_i}}{dI_{\text{Par}}^{VV}}\right|\Delta I_{\text{Par}}^{VV} + \left|\frac{dR_{J_i}}{dI_{\text{Perp}}^{HH}}\right|\Delta I_{\text{Perp}}^{HH} + \left|\frac{dR_{J_i}}{dn_{NG}}\right|\Delta n_{NG}, \tag{25}$$

(see Jones *et al.*[33]). The first six terms on the right hand side of Eq. (25) involve derivatives of $R_{J_i}$ with respect to the intensities appearing in the respective expressions for $R_{J_i}$ [left hand sides of Eqs. (22)–(24)], while the final term in Eq. (25), which represents the contribution to the total uncertainty due to uncertainty in the noble gas density, involves the derivative of $R_{J_i}$ [in the form of the right hand side of Eqs. (22), (23), or (24)] with respect to the noble gas density. The necessary derivatives are evaluated in Appendix B of the supplementary material, where we find [(B21), (B22), and (B24)]

$$\Delta R_{J_i=1(G^1\Pi_g)} = \left| \frac{\tilde{k}_{NG}^{J_i=1,M_i=0\to\pm1}}{\left(\tilde{k}_{NG}^{J_i=1,M_i=0\to\pm1} n_{NG} + C_1\right)} - \frac{\tilde{k}_{NG}^{Q}}{\left(1 + \tilde{k}_{NG}^{Q} n_{NG} + C_Q\right)} \right| \left( \frac{\tilde{k}_{NG}^{J_i=1,M_i=0\to\pm1} n_{NG} + C_1}{1 + \tilde{k}_{NG}^{Q} n_{NG} + C_Q} \right) \Delta n_{NG} + 6 \left| \frac{I^{\perp} + I^{\parallel}}{\left(2I^{\perp} - I^{\parallel}\right)^2} \right|_{\text{Probe } J_i=1\to G^1\Pi_g} (\Delta I), \quad (26)$$

$$\Delta R_{J_i=1\left(F^1\Sigma_g^+\right)} = \left| \frac{\tilde{k}_{NG}^{J_i=1,M_i=0\to\pm1}}{\left(\tilde{k}_{NG}^{J_i=1,M_i=0\to\pm1} n_{NG} + C_1\right)} - \frac{\tilde{k}_{NG}^{Q}}{\left(1 + \tilde{k}_{NG}^{Q} n_{NG} + C_Q\right)} \right| \left( \frac{\tilde{k}_{NG}^{J_i=1,M_i=0\to\pm1} n_{NG} + C_1}{1 + \tilde{k}_{NG}^{Q} n_{NG} + C_Q} \right) \Delta n_{NG} + 3 \left| \frac{I^{\perp} + I^{\parallel}}{\left(I^{\parallel}\right)^2} \right|_{\text{Probe } J_i=1\to F^1\Sigma_g^+} (\Delta I), \quad (27)$$

and

$$\Delta R_{J_i=3,5,7} = \left| \frac{\tilde{k}_{NG}^{J_i'=1\to J_i=3,5,7}}{\left(\tilde{k}_{NG}^{J_i'=1\to J_i=3,5,7} n_{NG} + C_{3,5,7}\right)} - \frac{\tilde{k}_{NG}^{Q}}{\left(1 + \tilde{k}_{NG}^{Q} n_{NG} + C_Q\right)} \right| \left( \frac{\left(\tilde{k}_{NG}^{J_i'=1\to J_i=3,5,7} n_{NG} + C_{3,5,7}\right)}{1 + \tilde{k}_{NG}^{Q} n_{NG} + C_Q} \right) \Delta n_{NG}$$
$$+ 9 \left| \frac{\left[2I^{\perp} + I^{\parallel}\right]_{\text{Probe } J_i=3,5,7\to G^1\Pi_g} + \left[2I^{\perp} + I^{\parallel}\right]_{\text{Probe } J_i'=1\to G^1\Pi_g}}{\left[2I^{\perp} + I^{\parallel}\right]^2_{\text{Probe } J_i'=1\to G^1\Pi_g}} \right| (\Delta I). \quad (28)$$

$\Delta I$ is determined from the measured background noise level of the signals. Contributions to the total uncertainty in individual data points due to the uncertainties in the measured intensities ranged from less than 1% up to 17% and from less than 2% up to 17% for the $M$-changing data obtained using the $G^1\Pi_g(v_e = 5, J_e = 1) \leftarrow A^1\Sigma_u^+(v_i = 5, J_i = 1)$ probe transition with argon and helium perturbers, respectively, from 10% to over 60% for the $M$-changing data obtained using the $F^1\Sigma_g^+(v_e = 12, J_e = 0) \leftarrow A^1\Sigma_u^+(v_i = 5, J_i = 1)$ probe transition with argon perturbers, and from less than 1% up to 27% and from 1% up to 17% for the $J$-changing data obtained using the $G^1\Pi_g(v_e = 5, J_e = J_i) \leftarrow A^1\Sigma_u^+(v_i = 5, J_i = 3, 5, 7)$ and $G^1\Pi_g\left(v_e = 5, J_e' = J_i'\right) \leftarrow A^1\Sigma_u^+\left(v_i = 5, J_i' = 1\right)$ probe transitions with argon and helium perturbers, respectively. As mentioned previously, the signals were very much smaller for studies of $M$-changing collisions using the $F^1\Sigma_g^+(v_e = 12, J_e = 0) \leftarrow A^1\Sigma_u^+(v_i = 5, J_i = 1)$ probe transition, which is why these uncertainties are so much larger and why we concentrated our measurements on those obtained using $G^1\Pi_g \leftarrow A^1\Sigma_u^+$ probe transitions. The uncertainty in the noble gas pressure was taken to be 0.2 Torr, based on the accuracy of the pressure gauge, the fact that the location of the gauge on the vacuum system was about 50 cm from the heat pipe oven, and because pressure measurements were not made in real time since the valve between the oven and the pressure gauge was closed during measurements. Since data were recorded using gas pressures that varied from 0.3 Torr to 30 Torr, this uncertainty was significant at low pressures, but fairly negligible at high pressures. The average uncertainty in the individual $R_{J_i=1(G^1\Pi_g)}$, $R_{J_i=1\left(F^1\Sigma_g^+\right)}$, and $R_{J_i=3,5,7}$ values introduced by the uncertainty in the noble gas density was ~5%.

Note that the contribution to the total uncertainty in a given data point, due to the uncertainty in noble gas density, depends on the fitted parameters, which in turn depend on the data (including the uncertainties). Thus, an iterative fitting process was used. Initial guesses for the values of the fitting parameters were used to calculate initial values of the error bars to be used in the first round of fitting. Parameter values obtained from this fit were then used to calculate revised error bars to use in the next round of fitting. This process was repeated until there was no further change in the fitted values or the error bars.

Initially, the values of the lithium parameters $C_i$ were allowed to vary in the fit. However, it was soon found that the error bars associated with the fitted $C_i$ values were very much larger than the values themselves. This is not surprising since the lithium atomic density was kept very low (~$5.0 \times 10^{13}$ cm$^{-3}$) so that we could isolate the noble gas collisions. If we assume that the lithium $J$-changing collision and quenching rate coefficients in units of Γ are similar in magnitude to those for potassium – NaK $A^1\Sigma^+(v = 16, J = 30)$ collisions determined by Jones *et al.*,[33] we estimate that $C_{1,3,5,7} \leq 0.0008$ and $C_Q \leq 0.014$ in the present case. Since the lowest measured values of $R_{J_i=1(G^1\Pi_g)}$, $R_{J_i=1\left(F^1\Sigma_g^+\right)}$, and $R_{J_i=3,5,7}$ are ~0.01, neglect of $C_{1,3,5,7}$ causes less than a 8% effect for data recorded at the lowest noble gas densities, and an even smaller effect at higher noble gas densities. Similarly, since the denominators of Eqs. (22)–(24) are always greater than 1, neglect of $C_Q$ causes less than 2% error.

Consequently, we set all of the $C_i$ values equal to zero in subsequent fits.

The results of our preliminary round of fitting yielded the parameter values given in Table C.1 of Appendix C of the supplementary material. The data are plotted against the fitting functions in Figs. C.1 and C.2 of Appendix C. The analysis supporting this fit explicitly made the assumption that all of the data were recorded in the "single collision regime." This assumption requires that the probability of more than one collision occurring within the excited state lifetime is negligible. As we can see from Fig. C.1 of Appendix C, this requirement appears to be satisfied reasonably well in our studies of $M$-changing collisions, where values of $n_{J_i=1,M_i=\pm1}/n_{J_i=1,M_i=0} < 0.1$, and hence the probability of two such collisions within the excited state lifetime is less than 0.01. This means that neglect of multiple collisions introduces less than a 10% error in the $M$-changing collision rate coefficient in this case.

However, as can be seen in Fig. C.2 of Appendix C, maximum values of $n_{J_i=3}/n_{J_i'=1}$, $n_{J_i=5}/n_{J_i'=1}$, and $n_{J_i=7}/n_{J_i'=1}$ are in the range 0.22–0.39, which certainly violates the single collision assumption since there is as much as 22–39% chance that a molecule that undergoes one $J$-changing collision will also undergo a second such collision before the excited state decays. The breakdown of the single collision approximation is also evident in the results listed in Table C.1. Quenching collisions include all collisions that depopulate a given level. Thus, the total quenching rate coefficient must be larger than the sum of all $J$-changing collision rate coefficients (including those corresponding to collisions that populate rotational levels that we did not study), plus smaller terms representing collisions that transfer population to other vibrational and electronic states. The fact that the sums of just the rate coefficients for $J$-changing collisions that populate $J_i = 3$, 5, and 7 from $J_i' = 1$ are larger than the quenching rate coefficients determined in the fit is a clear indication that neglect of multiple collision effects in the $J$-changing collision case is not warranted. A partial remedy for this problem is presented in Sec. III C 2.

### 2. Multiple collision corrections

In our single collision analysis, we considered population transfer from $J_i' = 1$ to $J_i = 3$, 5, and 7. However, we did not take into account back transfer to $J_i' = 1$ or multi-step transfer (from $J_i' = 1 \rightarrow J_i = 3 \rightarrow J_i = 7$, for example). However, as discussed in Sec. III C 1, the effects of multiple collisions are clearly significant for our studies of rotationally inelastic ($J$-changing) collisions. Mathematically, the effects of multiple collisions can be partially incorporated into the analysis by going back to Eq. (21), and retaining the multiple collision term involving the sum over $J$ but continuing to discard the terms corresponding to collisions with lithium atoms (since we have shown the latter to be negligible for all of our measurements):

$$\frac{n_{J_i=3,5,7}}{n_{J_i'=1}} = \frac{\left[2I^{\perp} + I^{\parallel}\right]_{\text{Probe } J_i=3,5,7\rightarrow G^1\Pi_g}}{\left[2I^{\perp} + I^{\parallel}\right]_{\text{Probe } J_i'=1\rightarrow G^1\Pi_g}} = \frac{\tilde{k}_{NG}^{J_i'=1\rightarrow J_i=3,5,7} n_{NG} + \sum_{J\neq 1,J_i}\left[\tilde{k}_{NG}^{J\rightarrow J_i=3,5,7} n_{NG}\right]\frac{n_J}{n_{J_i'=1}}}{1 + \tilde{k}_{NG}^{Q-J_i=3,5,7} n_{NG}}. \quad (29)$$

In this expression, the second term in the numerator recognizes the fact that, for example, level $J_i = 3$ can be populated by collisions of noble gas atoms with molecules in $J = 5$, 7, 9, 11,. . . (i.e., molecules in levels that were themselves collisionally populated), in addition to the single collision channel $J_i' = 1 \rightarrow J_i = 3$ (represented by the first term in the numerator).

Unfortunately, we have limited information on these multiple collision channels since our measurements did not involve direct excitation of levels other than $J_i' = 1$, and therefore we do not have a good first hand experimental estimate of terms like $k_{NG}^{J=5,7,9,11\rightarrow J_i=3}$. In the NaK experiments of Jones *et al.*,[33] the authors partially accounted for the effects of multiple collisions by making the assumption that, for a first order correction, an unknown rate coefficient could be replaced by a rate coefficient representing the same $\Delta J$. In that work, the rotational quantum number of the directly excited level was on the order of 30 and collisions with $|\Delta J|$ values up to ~20 were studied (including both positive and negative values of $\Delta J$). In the current work, we intentionally excited $J_i' = 1$ so that $M$-changing collisions could be studied directly. And since $\Delta J$ must be an even number for collisions involving homonuclear diatomic molecules, the only direct $J$-changing collisions that could be observed in the current experiment involved positive, even values of $\Delta J$. Therefore, in our multiple collision analysis, we make the assumption that $k_{NG}^{J=3\rightarrow J_i=5} = k_{NG}^{J=5\rightarrow J_i=7} = k_{NG}^{J_i'=1\rightarrow J_i=3}$ since these all correspond to $\Delta J = 2$ collisions, and $k_{NG}^{J=3\rightarrow J_i=7} = k_{NG}^{J_i'=1\rightarrow J_i=5}$ since these both correspond to $\Delta J = 4$. Rate coefficients for collisions involving negative values of $\Delta J$ were obtained from the principle of detailed balance,[61,62]

$$\frac{k^{i\rightarrow j}}{k^{j\rightarrow i}} = \frac{g_j}{g_i} e^{-(E_j - E_i)/kT}, \quad (30)$$

where the $g$ factors represent degeneracies and, in the present case, the exponential factor is ~1. From this, we calculate $k_{NG}^{J=5\rightarrow J_i=3} = (7/11)k_{NG}^{J=3\rightarrow J_i=5} = (7/11)k_{NG}^{J_i'=1\rightarrow J_i=3}$, $k_{NG}^{J=7\rightarrow J_i=5} = (11/15)k_{NG}^{J=5\rightarrow J_i=7} = (11/15)k_{NG}^{J_i'=1\rightarrow J_i=3}$, and $k_{NG}^{J=7\rightarrow J_i=3} = (7/15)k_{NG}^{J=3\rightarrow J_i=7} = (7/15)k_{NG}^{J_i'=1\rightarrow J_i=5}$.

The experimental intensity ratios in the middle expression of Eq. (29) provide values for the densities of the three levels ($J_i = 3$, 5, and 7) populated by $J$-changing collisions that were probed in the experiment, relative to that in the directly populated level $J_i' = 1$ [left side of Eq. (29)]. The right hand side of Eq. (29) contains these same ratios, $n_{J=3}/n_{J_i'=1}$, $n_{J=5}/n_{J_i'=1}$, and $n_{J=7}/n_{J_i'=1}$ (excluding $J = 1$, $J_i$), as well as ratios involving densities in higher $J$ levels (i.e., $n_{J=9}/n_{J_i'=1}$, $n_{J=11}/n_{J_i'=1}$, etc.). Our data provide values for the former group of ratios, but not for the latter group. Therefore, we truncate the sum in Eq. (29) at $J = 7$. In this context, it should be recognized that the first (single collision) term on the right hand side of Eq. (29) is the dominant contributor to the population in level $J_i$. And by including population transfer to $J_i$ from $J = 3$, 5, and 7 (which are the most heavily populated levels other than $J_i' = 1$), we are including the leading terms of the multiple collision correction. We believe that this procedure reduces any remaining error in the reported rate coefficients, due to incomplete multiple collision corrections, to less than 10%. We also expect that this remaining error is smallest for $J_i = 3$, where the single collision transfer of population corresponds to $\Delta J = 2$,

and the first neglected term (from the relatively weakly populated $J = 9$) corresponds to $\Delta J = -6$. Conversely, this remaining error is largest for $J_i = 7$, where single collision transfer corresponds to $\Delta J = 6$ and the first neglected term to $\Delta J = -2$ (although again the source of that first neglected term is the relatively weakly populated $J = 9$).

With the truncation of the sum in Eq. (29) to terms with $J \le 7$, that equation can be written in the form of three linear equations in three unknowns ($n_{J=3}/n_{J_i'=1}$, $n_{J=5}/n_{J_i'=1}$, and $n_{J=7}/n_{J_i'=1}$); see Appendix D of the supplementary material. These can be solved to yield the following equations (see Appendix D):

$$R_{J_i=3} = \frac{\left[2I^{\perp} + I^{\parallel}\right]_{\text{Probe } J_i=3\to G^1\Pi_g}}{\left[2I^{\perp} + I^{\parallel}\right]_{\text{Probe } J_i'=1\to G^1\Pi_g}} = \left[\frac{165Q^2 z_{13} + 105Q z_{13} z_{15} + 77Q z_{15} z_{17} - 121 z_{13}^3 + 77 z_{13}^2 z_{17} + 77 z_{13} z_{15}^2}{165Q^3 - 226Q z_{13}^2 - 77Q z_{15}^2 - 154 z_{13}^2 z_{15}}\right], \tag{31}$$

$$R_{J_i=5} = \frac{\left[2I^{\perp} + I^{\parallel}\right]_{\text{Probe } J_i=5\to G^1\Pi_g}}{\left[2I^{\perp} + I^{\parallel}\right]_{\text{Probe } J_i'=1\to G^1\Pi_g}} = \left[\frac{165Q^2 z_{15} + 165Q z_{13}^2 + 121Q z_{13} z_{17} + 121 z_{13}^2 z_{15} + 77 z_{13} z_{15} z_{17} - 77 z_{15}^3}{165Q^3 - 226Q z_{13}^2 - 77Q z_{15}^2 - 154 z_{13}^2 z_{15}}\right], \tag{32}$$

and

$$R_{J_i=7} = \frac{\left[2I^{\perp} + I^{\parallel}\right]_{\text{Probe } J_i=7\to G^1\Pi_g}}{\left[2I^{\perp} + I^{\parallel}\right]_{\text{Probe } J_i'=1\to G^1\Pi_g}} = \left[\frac{165Q^2 z_{17} + 330Q z_{13} z_{15} + 165 z_{13}^3 - 105 z_{13}^2 z_{17} + 105 z_{13} z_{15}^2}{165Q^3 - 226Q z_{13}^2 - 77Q z_{15}^2 - 154 z_{13}^2 z_{15}}\right], \tag{33}$$

where we have introduced the shorthand notation $z_{13} \equiv \left(\tilde{k}_{NG}^{J_i'=1\to J_i=3} n_{NG}\right)$, $z_{15} \equiv \left(\tilde{k}_{NG}^{J_i'=1\to J_i=5} n_{NG}\right)$, $z_{17} \equiv \left(\tilde{k}_{NG}^{J_i'=1\to J_i=7} n_{NG}\right)$, and $Q \equiv \left(1 + \tilde{k}_{NG}^{Q} n_{NG}\right)$. It should be noted that Eqs. (31)–(33) can be expanded in powers of $n_{NG}$ (which are contained in the parameters $z_{13}$, $z_{15}$, $z_{17}$, and $Q$). The leading terms of these expansions are just the linear (single collision) terms in Eq. (24). We chose not to work with the power series expansions since the "exact" solutions, (31)–(33), were straightforward to implement in the fitting routine.

Equations (31)–(33) for the $J$-changing data obtained using $G^1\Pi_g(v_e = 5, J_e = J_i) \leftarrow A^1\Sigma_u^+(v_i = 5, J_i = 3, 5, 7)$ and $G^1\Pi_g\left(v_e = 5, J'_e = J_i'\right) \leftarrow A^1\Sigma_u^+\left(v_i = 5, J_i' = 1\right)$ probe transitions, along with Eqs. (22) and (23) for the $M$-changing data obtained using $G^1\Pi_g(v_e = 5, J_e = 1) \leftarrow A^1\Sigma_u^+(v_i = 5, J_i = 1)$ and $M$-changing

**TABLE I.** Final values of rate coefficients ($k_{Ar,He}^{J_i=1,M_i=0\to\pm1}$ and $k_{Ar,He}^{J_i'=1\to J_i=3,5,7}$) divided by the radiative rate $\Gamma$ and in units of cm$^3$ s$^{-1}$ [the latter obtained by multiplying the fitted parameters ($\tilde{k}_{Ar,He}^{J_i=1,M_i=0\to\pm1}$ and $\tilde{k}_{Ar,He}^{J_i'=1\to J_i=3,5,7}$) by $\Gamma = 5.45 \times 10^7$ s$^{-1}$ [63]] for $M$-changing (elastic) collisions, $A^1\Sigma_u^+(v_i = 5, J_i = 1, M_i = 0) \to A^1\Sigma_u^+(v_i = 5, J_i = 1, M_i = \pm1)$, and for $J$-changing (inelastic) collisions, $A^1\Sigma_u^+\left(v_i = 5, J_i' = 1\right) \to A^1\Sigma_u^+(v_i = 5, J_i = 3, 5, 7)$, of $Li_2$ molecules with argon and helium atoms. Quenching rate coefficients are also given. Note that these results are based on the model that partially takes multiple collision effects into account in the analysis of the $J$-changing collision data. Quoted uncertainties represent statistical errors only. We believe realistic uncertainties in all rate coefficients are on the order of 10% due to the failure to completely account for multiple collision effects.

| $M$-changing | $\tilde{k}_{Ar}^{J_i=1,M_i=0\to\pm1}$ ($10^{-18}$ cm$^3$) | $\tilde{k}_{He}^{J_i=1,M_i=0\to\pm1}$ ($10^{-18}$ cm$^3$) | $k_{Ar}^{J_i=1,M_i=0\to\pm1}$ ($10^{-11}$ cm$^3$ s$^{-1}$) | $k_{He}^{J_i=1,M_i=0\to\pm1}$ ($10^{-11}$ cm$^3$ s$^{-1}$) |
|---|---|---|---|---|
| $J_i = 1, M_i = 0 \to J_i = 1, M_i = \pm1$ | 1.64 ± 0.05 | 1.09 ± 0.04 | 8.95 ± 0.25 | 5.92 ± 0.22 |
| $J$-changing | $\tilde{k}_{Ar}^{J_i'=1\to J_i=3,5,7}$ ($10^{-18}$ cm$^3$) | $\tilde{k}_{He}^{J_i'=1\to J_i=3,5,7}$ ($10^{-18}$ cm$^3$) | $k_{Ar}^{J_i'=1\to J_i=3,5,7}$ ($10^{-11}$ cm$^3$ s$^{-1}$) | $k_{He}^{J_i'=1\to J_i=3,5,7}$ ($10^{-11}$ cm$^3$ s$^{-1}$) |
| $J_i' = 1 \to J_i = 3$ | 6.82 ± 0.20 | 4.77 ± 0.19 | 37.2 ± 1.1 | 26.0 ± 1.0 |
| $J_i' = 1 \to J_i = 5$ | 2.56 ± 0.11 | 3.44 ± 0.15 | 14.0 ± 0.6 | 18.8 ± 0.8 |
| $J_i' = 1 \to J_i = 7$ | 2.56 ± 0.10 | 3.26 ± 0.14 | 14.0 ± 0.6 | 17.7 ± 0.8 |
| Quenching | $\tilde{k}_{Ar}^{Q}$ ($10^{-18}$ cm$^3$) | $\tilde{k}_{He}^{Q}$ ($10^{-18}$ cm$^3$) | $k_{Ar}^{Q}$ ($10^{-11}$ cm$^3$ s$^{-1}$) | $k_{He}^{Q}$ ($10^{-11}$ cm$^3$ s$^{-1}$) |
| | 17.3 ± 0.7 | 17.5 ± 0.9 | 94.2 ± 3.7 | 95.2 ± 5.1 |

data obtained using $F^1\Sigma_g^+(v_e = 12, J_e = 0) \leftarrow A^1\Sigma_u^+(v_i = 5, J_i = 1)$ probe transitions, respectively, served as the fitting functions in the analysis including multiple collision corrections.

Again, we used the nonlinear multiple regression tool of Origin version 9.3 (2016) to simultaneously fit the $M$-changing collision and $J$-changing collision data collected using either argon or helium as the buffer gas. For each data point, the independent variables are again the noble gas type (either argon or helium), the noble gas density [which is buried inside the factors $z_{13}$, $z_{15}$, $z_{17}$, and $Q$ in Eqs. (31)–(33)], and the relevant $J_i$ level, while the dependent variable is the left hand side of Eqs. (22), (23), (31), (32), or (33) obtained from the measured fluorescence intensities. And again, the fitting parameters are the ten rate coefficients (i.e.; $\tilde{k}_{Ar}^{J_i=1,M_i=0\rightarrow\pm1}$, $\tilde{k}_{He}^{J_i=1,M_i=0\rightarrow\pm1}$, $\tilde{k}_{Ar}^{J_i'=1\rightarrow J_i=3}$, $\tilde{k}_{He}^{J_i'=1\rightarrow J_i=3}$, $\tilde{k}_{Ar}^{J_i'=1\rightarrow J_i=5}$, $\tilde{k}_{He}^{J_i'=1\rightarrow J_i=5}$, $\tilde{k}_{Ar}^{J_i'=1\rightarrow J_i=7}$, $\tilde{k}_{He}^{J_i'=1\rightarrow J_i=7}$, $\tilde{k}_{Ar}^{Q}$ and $\tilde{k}_{He}^{Q}$). The lithium parameters $C_1$, $C_3$, $C_5$, $C_7$, and $C_Q$ are again all set to zero. Error bars for the $M$-changing data are the same as in the single collision analysis. Error bars for the $J$-changing data are determined using the same techniques as used in the single collision analysis of the $J$-changing data, although the expressions are much more complicated. The details of these error bar calculations are given in Appendix E of the supplementary material.

The results of this fit are given in Table I and the fitted functions are plotted against the data in Figs. 6 and 7.

As can be seen in Fig. 6 or Fig. C1, there is a fairly small, but clear systematic discrepancy between our $M$-changing data obtained using $G^1\Pi_g(v_e = 5, J_e = 1) \leftarrow A^1\Sigma_u^+(v_i = 5, J_i = 1)$ probe transitions and $M$-changing data obtained using $F^1\Sigma_g^+(v_e = 12, J_e = 0) \leftarrow A^1\Sigma_u^+(v_i = 5, J_i = 1)$ probe transitions. We have not yet been able to discover the origin of this discrepancy, and consequently, we felt that both datasets should be included in the fits. However, the error bars associated with the $F$ state data are so much larger than those associated with the $G$ state data that the former have relatively little impact on the fits. Specifically, we found that the elimination of all $F$ state data leads to an increase in the argon rate coefficients, $k_{Ar}^{J_i=1,M_i=0\rightarrow\pm1}$ and $k_{Ar}^{Q}$ of less than 1.4%, an increase in the argon $J$-changing rate coefficients $k_{Ar}^{J_i'=1\rightarrow J_i=3,5,7}$ (which are correlated with $k_{Ar}^{Q}$) of less than 1%, and of course no effect on the helium rate coefficients.

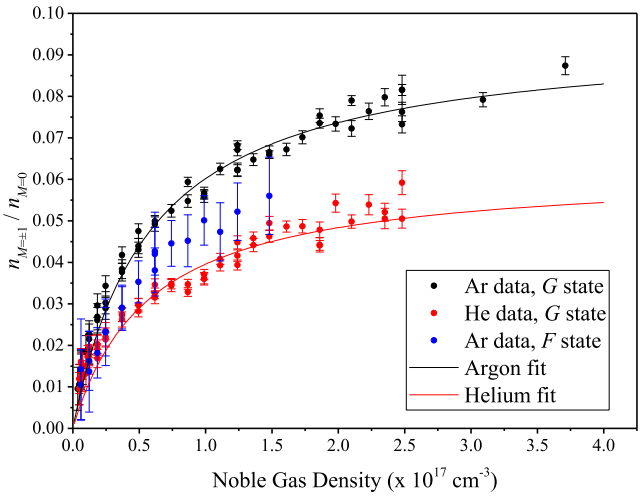


**FIG. 6**. Data and fitting function for elastic ($M$-changing) collisions of $Li_2$ $A^1\Sigma_u^+(v_i = 5, J_i = 1)$ molecules with noble gas atoms. The plot shows the density in either collisionally populated level $J_i$ = 1, $M_i$ = +1 or $J_i$ = 1, $M_i$ = −1 divided by the density in the directly excited level $J_i$ = 1, $M_i$ = 0 vs noble gas density. Black and red data points were recorded using the $G^1\Pi_g(v_e = 5, J_e = J_i = 1) \leftarrow A^1\Sigma_u^+(v_i = 5, J_i = 1)$ probe transition with argon or helium buffer gas, respectively. Blue data points were recorded using the $F^1\Sigma_g^+(v_e = 12, J_e = 0) \leftarrow A^1\Sigma_u^+(v_i = 5, J_i = 1)$ probe transition with argon buffer gas. The black curve is a fit to all argon data (including both probe transitions), while the red curve is a fit to the helium data. These fits were obtained using the analysis that includes multiple collision corrections.

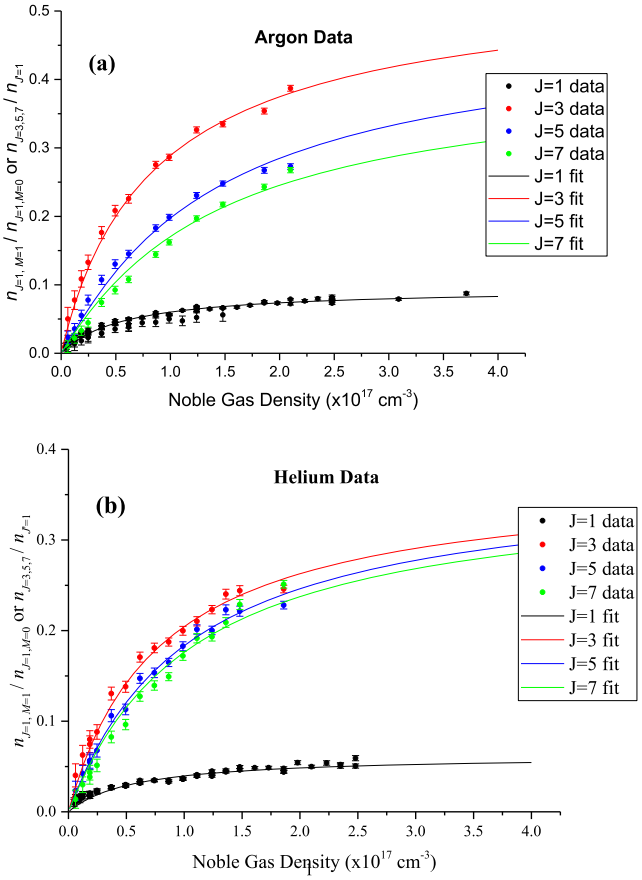


**FIG. 7**. Data and fitting function for elastic ($M$-changing) and inelastic ($J$-changing) collisions of $Li_2$ $A^1\Sigma_u^+(v_i = 5, J_i = 1)$ molecules with noble gas atoms. The black data points show the density in either collisionally populated level $J_i$ = 1, $M_i$ = +1 or $J_i$ = 1, $M_i$ = −1 divided by the density in the directly excited level $J_i$ = 1, $M_i$ = 0 vs noble gas density. Red, blue, and green data points show the density in the collisionally populated levels $J_i$ = 3, 5, or 7, respectively, divided by the density in the directly excited level $J_i' = 1$ vs noble gas density. The black, red, blue, and green solid lines represent fits obtained using the analysis that includes multiple collision corrections. (a) Argon data; (b) Helium data.

## IV. CONCLUSIONS

The most interesting result of the present work is the fact that the elastic $M$-changing collision rate is more than a factor of four times smaller than the inelastic, $\Delta J = +2$, $J$-changing collision rate for collisions of $Li_2$ $A^1\Sigma_u^+(v = 5, J = 1)$ molecules with either argon or helium atoms. In other words, it is significantly more difficult for a collision with a noble gas atom to change the orientation of the molecular rotation vector than to change the magnitude of the rotation vector. These results are consistent with, but extend, the measurements of Wolfe *et al.*[32] and Jones *et al.*[33] In both of these previous studies, the authors looked at changes of rotational quantum number $J$, and destruction of orientation, in inelastic collisions of NaK $A^1\Sigma^+$ molecules with argon, helium, and potassium atoms. Those authors found that $J$-changing collisions of NaK $A^1\Sigma^+$ molecules with argon atoms resulted in the destruction of roughly half of the initial orientation, while the same type of collisions with helium atoms preserved most of the initial orientation, and collisions with potassium atoms destroyed almost all of the initial orientation. However, the experiments of Wolfe *et al.* and Jones *et al.* only looked at inelastic collisions; i.e., what fraction of the initial orientation is lost in a single collision that resulted in a change of rotational quantum number by a particular amount. In addition, since the initial rotational quantum numbers were in the range of 14–44 in those previous works, it was not possible to study individual initial and final $M$ levels, but rather only the overall average orientation that remained after a particular type of $J$-changing collision.

The present work provides a quantitative measurement of the rate coefficient for transfer of population between $M$ levels of the $Li_2$ $A^1\Sigma_u^+(v = 5, J = 1)$ state in collisions with argon and helium atoms. In this case, it was possible to isolate a specific $A^1\Sigma_u^+(v_i = 5, J_i = 1, M_i = 0) \rightarrow A^1\Sigma_u^+(v_i = 5, J_i = 1, M_i = \pm 1)$ collision channel by choosing the initial level as $J_i = 1$, $M_i = 0$. In this sense, our work is directly comparable to the early works of Silvers *et al.*[50] and Borkenhagen *et al.*[34] In the work of Silvers *et al.*, the $J_i = 1$, $M_i = 0$ level of the BaO $A^1\Sigma^+(v_i = 1)$ state was populated from $X^1\Sigma^+(v_g = 0, J_g = 0, M_g = 0)$ with a linearly polarized laser. The probe laser tuned to the $C^1\Sigma^+(v_e = 3, J_e = 0) \leftarrow A^1\Sigma^+(v_i = 1, J_i = 1)$ transition sampled the population in the directly excited level $[A^1\Sigma^+(v_i = 1, J_i = 1, M_i = 0)]$, if its polarization vector was parallel to that of the pump laser, or the population in the collisionally populated levels $[A^1\Sigma^+(v_i = 1, J_i = 1, M_i = \pm 1)]$, if its polarization vector was perpendicular to that of the pump laser. The measured upper state fluorescence ratio $I^{\perp}/I^{\parallel}$ then yielded the population ratio $n_{J_i=1,M_i=\pm 1}/n_{J_i=1,M_i=0}$. This is completely analogous to our measurements of $M$-changing collisions with the $F^1\Sigma_g^+(v_e = 12, J_e = 0) \leftarrow A^1\Sigma_u^+(v_i = 5, J_i = 1)$ probe. Silvers *et al.* found no detectable signals representing $M$-changing collisions for BaO $A^1\Sigma^+(v_i = 1, J_i = 1)$ molecules colliding with argon (but set an upper limit for the cross section of 1 Å$^2$ for such transitions). However, they did detect $M$-changing collisions for BaO $A^1\Sigma^+(v_i = 1, J_i = 1)$ molecules colliding with $CO_2$ molecules and determined a cross section of 4.2 ± 1.2 Å$^2$. Borkenhagen *et al.*,[34] using a molecular beam-electric resonance method, determined $X^1\Sigma^+(v = 0, J = 1, M = 1) \rightarrow X^1\Sigma^+(v = 0, J = 1, M = 0)$ $M$-changing collision cross sections of 4.1 ± 3 Å$^2$, 5 ± 4 Å$^2$, and 7 ± 4 Å$^2$ for CsF molecules colliding with Ne, Ar, and Kr atoms. Our measured $M$-changing rate coefficients for $Li_2$ $A^1\Sigma_u^+(v_i = 5, J_i = 1)$ molecules can be converted to cross sections of 7.1 Å$^2$ and 2.6 Å$^2$ for argon and helium, respectively. These values are somewhat larger than the upper limit established by the null result of Silvers *et al.* for BaO $A^1\Sigma^+(v_i = 1, J_i = 1)$ collisions with argon and completely comparable in magnitude to the results of Borkenhagen *et al.*

The rate coefficients for $J$-changing collisions of $Li_2$ molecules in the $A^1\Sigma_u^+(v = 5, J = 1)$ state with argon determined in the present work are very close in magnitude to those reported by Scott *et al.*[11] for collisions of $Li_2$ $A^1\Sigma_u^+(v = 9, J = 8)$ with argon atoms. Scott *et al.* demonstrated that rotationally inelastic rate coefficients drop slowly with the increasing initial $J$ value and are not strongly dependent on the noble gas collision partner. In particular, our rate coefficients for $J$-changing collisions of $Li_2$ $A^1\Sigma_u^+(v = 5, J = 1)$ with both argon and helium atoms are close in magnitude (roughly a factor of two larger) to those reported by Stewart and co-workers[15–18] for collisions of $Li_2$ $A^1\Sigma_u^+(v = 2, 5, 6, 7, 12, 17, 24, J = 30)$ and $A^1\Sigma_u^+(v = 0, J = 18)$ with neon. Our measured $J$-changing collision rate coefficients are also roughly a factor of two larger, and our quenching rate coefficients are comparable in magnitude to those determined by Wolfe *et al.*[32] and Jones *et. al.*[33] for collisions of argon and helium atoms with NaK molecules in the $A^1\Sigma^+$ state. Each of these previous measurements involved much higher initial state rotational quantum numbers (14–44) than was studied in the present work (where $J_i = 1$ always).

Comparison of our results to those of other experiments is somewhat limited by the fact that collision velocities are dependent on temperature, which varies from one study to another, and because the narrowband lasers used in the present work primarily excite those molecules with zero velocity component along the laser propagation axis, whereas all velocity groups are excited in experiments using broadband lasers. However, mean velocities scale only as the square root of temperature, and all experiments are carried out at absolute temperatures that are within roughly a factor of two of each other. In addition, although one component of the molecular velocity is selected, the other two are not, and neither is any of the three velocity components of the atomic collision partner. Therefore, we do not believe that differences in collisional speed distributions are as significant in our comparison to previous studies as differences in the molecule under investigation, the atomic collision partner, or the initial rotational quantum number. Nevertheless, we note that the rate coefficients measured in the current work are all of the same magnitude as those measured in other experiments for similar collisional processes.

We note that there is an advantage to studying both elastic and inelastic collisions and analyzing the results simultaneously. In general, the $J$-changing collision data are much cleaner than the $M$-changing collision data because the $J$-changing collision rates are much larger than the $M$-changing rates. However, both sets of data also depend on the quenching rate coefficients. Therefore, the $J$-changing data help pin down a more accurate determination of the quenching coefficients, which, in turn, helps in providing more accurate values for the $M$-changing rate coefficients (and vice versa).

It is also interesting to note that, just as in the work of Jones *et al.*,[33] the effects of multiple collisions must be taken into account in order to obtain reasonably accurate rate coefficients. A clear signature of this is the fact that, in the absence of multiple collision

corrections, the sum of the fitted $J$-changing collision rate coefficients for $\Delta J = 2$, 4, and 6 is larger than the fitted quenching rate coefficient (which should equal this sum plus a number of other positive terms); see Table C.1 of the supplementary material. However, there are a number of differences between our current implementation of multiple collision corrections and that used by Jones *et al.*

In the experiment of Jones *et al.*, the authors pumped initial rotational levels around $J = 30$ and observed collisional transitions out to around $\Delta J = \pm 20$. The number of rate coefficients to describe all collisional transitions between these levels is very high and solving the rate equations would have been difficult. Moreover, because the fitting parameters are correlated and because there were no measurements that gave first order information relating to many of these parameters, there was no way to successfully fit with that many rate coefficients. Consequently, the authors made several approximations to simplify their model. First, they assumed that rate coefficients for equivalent values of $\Delta J$ are equal to each other. In this way, all multiple collision events could be described in terms of the primary rate coefficients for each $\Delta J$ value starting from the initially excited level. However, even with this major simplification, it still was not possible to develop a fitting function that would incorporate all of the multiple collision processes and successfully fit the data. Instead, the authors carried out a fit based on the single-collision model and then afterward made a "worst case" correction assuming that all data had been recorded at the highest pressures where multiple collision effects are most important. In this way, they were able to estimate an upper limit to the magnitude of neglected multiple collision effects.

The present approach to the multiple collision corrections has both advantages and disadvantages compared to that used by Jones *et al.* Jones *et al.* were able to include many levels in their multiple collision analysis, and had direct measurements corresponding to both positive and negative $\Delta J$ values. In addition, the initial pumped level was in the range $J = 14$–44, so energy gaps between rotational levels, and degeneracy factors for neighboring levels, are more nearly equal. Hence, the approximation that rate coefficients for equivalent values of $\Delta J$ are equal to each other is likely to be fairly good. In the present case, we are dealing with very low rotational quantum numbers, so energy gaps and degeneracy factors are less nearly equal and we also do not have any direct information on collisions with negative $\Delta J$ values. All of the energy gaps are small, relative to $kT$, so we do not think that differences in these values are likely to cause much difference in the rate coefficients, but the degeneracy factors might. We partially take the degeneracy factors into account by employing the principle of detailed balance to evaluate rate coefficients for negative $\Delta J$ in terms of those for positive $\Delta J$.

In the present work, we only include three collisionally populated rotational levels in the analysis ($J = 3$, 5, and 7). Hence, if we limit the multiple collision corrections to population transfer originating from those three levels, the number of rate coefficients is manageable. Consequently, we were able to solve the rate equations analytically and develop a fitting function that takes these multiple collision events into account for each data point at each noble gas pressure. Therefore, in this case, we are not just getting an upper limit on the effects of multiple collisions, but rather an exact accounting of collisional transfer processes originating from these three levels. This is the main advantage of our current analysis compared to that of Jones *et al.* The main disadvantage in our present multiple collision correction is that we cannot incorporate contributions from $J$ levels above $J = 7$. Consequently, our correction for $J = 3$ is pretty good, our correction for $J = 5$ is somewhat less good, and our correction for $J = 7$ is the least good. For $J = 3$, we include multiple collision processes involving $\Delta J = -2$ and $\Delta J = -4$ in the final step, while the largest missing contribution is from $\Delta J = -6$ collisions originating in the first neglected level $J = 9$. Conversely, for $J = 7$, we include the effects of multiple collision events involving $\Delta J = +2$ and $\Delta J = +4$ in the final step, but miss contributions from $\Delta J = -2, -4, \ldots$ collisions starting from levels $J \geq 9$. However, we note that levels $J \geq 9$ are much less populated than levels $J = 3$ and $J = 5$.

Finally, we note that we do not include multiple collision processes in our analysis of the $M$-changing collisions $J_i = 1, M_i = 0 \rightarrow J_i = 1, M_i = \pm 1$. In principle, the $J_i = 1, M_i = \pm 1$ levels can be populated by multiple collision processes such as $J_i' = 1, M_i' = 0 \rightarrow J_i = 3 \rightarrow J_i = 1, M_i = \pm 1$. Unfortunately, we are unable to estimate the magnitude of such contributions since our data do not provide information on changes of $M$ that occur in inelastic $J$-changing collisions. However, our data, combined with those of Wolfe *et al.* and Jones *et al.*, do indicate that $M$ changes are much less likely than $J$ changes. Consequently, the majority of $J_i' = 1, M_i' = 0 \rightarrow J_i = 3 \rightarrow J_i = 1$ processes are likely to repopulate $M_i = 0$, rather than $M_i = \pm 1$.

If we compare the rate coefficients listed in Table I in this paper with those listed in Table C.1 of the supplementary material, we see that the largest effects of the multiple collision corrections are to raise the values of the quenching rate coefficients and to reduce the values of the $J$-changing rate coefficients, especially for $J = 5$ and $J = 7$. The corrections are quite small for $J = 3$ since this level is populated most strongly by single collision events originating in $J = 1$. In the single collision approximation, the rate coefficients $k_{NG}^{J_i'=1\rightarrow J_i=3,5,7}$ are determined by the slopes of the $n_{J_i=3,5,7}/n_{J_i'=1}$ curves in Figs. 7(a) and 7(b) at low noble gas densities [see Eq. (24)], and the high density plateau regions of these curves yield the ratios $k_{NG}^{J_i'=1\rightarrow J_i=3,5,7}/k_{NG}^{Q}$. In the analysis that includes multiple collision effects, the rate coefficients, $k_{NG}^{J_i'=1\rightarrow J_i=3,5,7}$, are still determined by the slopes of the $n_{J_i=3,5,7}/n_{J_i'=1}$ curves in Figs. 7(a) and 7(b) at low noble gas densities because these data are only very slightly affected by multiple collision corrections. However, the high density plateau regions of the $n_{J_i=3,5,7}/n_{J_i'=1}$ curves in Figs. 7(a) and 7(b) are now given by $\left[k_{NG}^{J_i'=1\rightarrow J_i=3,5,7} + \sum_{J\neq 1,J_i} k_{NG}^{J\rightarrow J_i=3,5,7}\frac{n_J}{n_{J_i'=1}}\right]/k_{NG}^{Q}$ [see Eq. (29)]. The extra terms in the numerator effectively increase the $k_{NG}^{Q}$ values. Even though the $M$-changing data are not corrected for multiple collision effects, in this final fit, we do obtain revised values for the $M$-changing collisional rate coefficients associated with these increases in the $k_{NG}^{Q}$ values. Thus, the multiple collision correction for the $J$-changing collision analysis also leads to improved values of the $M$-changing collisional rate coefficients.

Finally, one can reasonably ask whether it might be preferable to limit the $J$-changing data to lower pressure data points only, and then dispense with the multiple collision correction altogether. To test this, we carried out a series of single collision model fits in which we excluded the inelastic collision data corresponding to noble gas pressures above a specified cutoff pressure. Specific values of 10 Torr,

7 Torr, 5 Torr, and 3 Torr for the cutoff pressure were chosen. The results of these fits are presented in Appendix F of the supplementary material, where we see that the new fits yield rate coefficients that are similar in magnitude to those obtained with our multiple collision model, but with larger error bars that increase in size as the cutoff pressure is reduced. Part of this is due to the fact that the relative uncertainty in the pressure measurement is largest at lower pressures and we also expect statistical uncertainties to increase with reduction of the size of the dataset. In addition, the neglected lithium contributions become more significant at the lowest noble gas pressures. However, as mentioned above, the high density plateau regions of the $n_{J=3,5,7}/n_{J'=1}$ curves obtained with the model that includes the multiple collision corrections are important for the accurate determination of the quenching coefficients. The quenching coefficients in turn are important since they still influence the fits at pressures of even a few Torr. The single collision model fitted quenching rate coefficients systematically increase as the cutoff pressure is reduced, and these quenching rate coefficients only exceed the sum of the three reported $J$-changing collision rate coefficients for the lowest two cutoff pressures, 5 Torr and 3 Torr. Thus, we believe that multiple collision effects still play a non-negligible role at pressures of just a few Torr, and hence that our fits including multiple collision corrections provide the most accurate results we have obtained from our data. These results are presented in Table I.

## SUPPLEMENTARY MATERIAL

See the supplementary material for Appendixes A–F mentioned in the text. Appendix A presents details related to the determination of level densities in terms of measured fluorescence signals. Appendix B discusses error analysis related to the single collision approximation model. Appendix C presents results of the single collision approximation model. Details of the multiple collision corrections are given in Appendix D, and error analysis results associated with the multiple collision correction model are given in Appendix E. Appendix F presents results based on single collision model analysis of various datasets in which the data corresponding to high noble gas pressures were eliminated.

## ACKNOWLEDGMENTS

This work was supported by the National Science Foundation (Grant Nos. PHY 1607432 and PHY 1912269) at Temple University, the Lagerqvist Research Fund of Temple University, and by the National Science Foundation (Grant No. PHY 1403060) at Lehigh University. We thank Dr. Teri Price for useful discussions.

## DATA AVAILABILITY

The data that support the findings of this study are available from the corresponding author upon reasonable request.

## REFERENCES

[1]H. Salami, T. Bergeman, B. Beser, J. Bai, E. H. Ahmed, S. Kotochigova, A. M. Lyyra, J. Huennekens, C. Lisdat, A. V. Stolyarov, O. Dulieu, P. Crozet, and A. J. Ross, Phys. Rev. A **80**, 022515 (2009).
[2]J. M. Bai, E. H. Ahmed, B. Beser, Y. Guan, S. Kotochigova, A. M. Lyyra, S. Ashman, C. M. Wolfe, J. Huennekens, F. Xie, D. Li, L. Li, M. Tamanis, R. Ferber, A. Drozdova, E. Pazyuk, A. V. Stolyarov, J. G. Danzl, H. C. Nägerl, N. Bouloufa, O. Dulieu, C. Amiot, H. Salami, and T. Bergeman, Phys. Rev. A **83**, 032514 (2011).
[3]S. Ashman, B. McGeehan, C. M. Wolfe, C. Faust, K. Richter, J. Jones, A. P. Hickman, and J. Huennekens, J. Chem. Phys. **136**, 114313 (2012).
[4]C. Ottinger, R. Velasco, and R. N. Zare, J. Chem. Phys. **52**, 1636 (1970).
[5]C. Ottinger and D. Poppe, Chem. Phys. Lett. **8**, 513 (1971).
[6]G. Ennen and C. Ottinger, Chem. Phys. **3**, 404 (1974).
[7]M. D. Rowe and A. J. McCaffery, Chem. Phys. **34**, 81 (1978).
[8]M. D. Rowe and A. J. McCaffery, Chem. Phys. **43**, 35 (1979).
[9]C. Ottinger and M. Schröder, J. Phys. B: At., Mol. Opt. Phys. **12**, 3533 (1979).
[10]C. Ottinger and M. Schröder, J. Phys. B: At., Mol. Opt. Phys. **13**, 4163 (1980).
[11]T. P. Scott, N. Smith, and D. E. Pritchard, J. Chem. Phys. **80**, 4841 (1984).
[12]B. Stewart, P. D. Magill, T. P. Scott, J. Derouard, and D. E. Pritchard, Phys. Rev. Lett. **60**, 282 (1988).
[13]P. D. Magill, T. P. Scott, N. Smith, and D. E. Pritchard, J. Chem. Phys. **90**, 7195 (1989).
[14]B. Stewart, P. D. Magill, and D. E. Pritchard, J. Phys. Chem. A **104**, 10565 (2000).
[15]Y. Gao and B. Stewart, J. Chem. Phys. **103**, 860 (1995).
[16]Y. Gao, P. S. Gorgone, S. Davis, E. K. McCall, and B. Stewart, J. Chem. Phys. **104**, 1415 (1996).
[17]B. A. Stewart, T. N. Stephens, B. A. Lawrence, and G. C. McBane, J. Phys. Chem. A **114**, 9875 (2010).
[18]M. Rosenberry, R. Marhatta, and B. Stewart, Chem. Phys. Lett. **523**, 15 (2012).
[19]K. Bergmann and W. Demtröder, J. Phys. B: At. Mol. Phys. **5**, 1386 (1972).
[20]K. Bergmann and W. Demtröder, J. Phys. B: At. Mol. Phys. **5**, 2098 (1972).
[21]K. Bergmann, W. Demtröder, M. Stock, and G. Vogl, J. Phys. B: At., Mol. Opt. Phys. **7**, 2036 (1974).
[22]R. Feinberg, R. E. Teets, J. Rubbmark, and A. L. Schawlow, J. Chem. Phys. **66**, 4330 (1977).
[23]P. L. Jones, U. Hefter, A. Mattheus, J. Witt, K. Bergmann, W. Müller, W. Meyer, and R. Schinke, Phys. Rev. A **26**, 1283 (1982).
[24]R. B. Kurzel, J. I. Steinfeld, D. A. Hatzenbuhler, and G. E. Leroi, J. Chem. Phys. **55**, 4822 (1971).
[25]R. Clark and A. J. McCaffery, Mol. Phys. **35**, 617 (1978).
[26]S. R. Jeyes, A. J. McCaffery, and M. D. Rowe, Mol. Phys. **36**, 845 (1978).
[27]M. A. A. Clyne, M. C. Heaven, and S. J. Davis, J. Chem. Soc., Faraday Trans. II **76**, 961 (1980).
[28]L. J. Van de Burgt and M. C. Heaven, Chem. Phys. **103**, 407 (1986).
[29]G. Sha, D. Proch, and K. L. Kompa, J. Chem. Phys. **87**, 5251 (1987).
[30]C. Ottinger, Chem. Phys. **1**, 161 (1973).
[31]J. McCormack and A. J. McCaffery, Chem. Phys. **51**, 405 (1980).
[32]C. M. Wolfe, S. Ashman, J. Bai, B. Beser, E. H. Ahmed, A. M. Lyyra, and J. Huennekens, J. Chem. Phys. **134**, 174301 (2011).
[33]J. Jones, K. Richter, T. J. Price, A. J. Ross, P. Crozet, C. Faust, R. F. Malenda, S. Carlus, A. P. Hickman, and J. Huennekens, J. Chem. Phys. **147**, 144303 (2017).
[34]U. Borkenhagen, H. Malthan, and J. P. Toennies, J. Chem. Phys. **71**, 1722 (1979).
[35]M. Yang, M. H. Alexander, H. J. Werner, J. Hohmann, L. Neitsch, F. Stuhl, and P. J. Dagdigian, J. Chem. Phys. **102**, 4069 (1995).
[36]O. Nédélec and J. Dufayard, J. Chem. Phys. **76**, 378 (1982).
[37]B. Nizamov and P. J. Dagdigian, J. Chem. Phys. **113**, 4124 (2000).
[38]C. J. Eyles, M. Brouard, C.-H. Yang, J. Kłos, F. J. Aoiz, A. Gijsbertsen, A. E. Wiskerke, and S. Stolte, Nat. Chem. **3**, 597 (2011).
[39]J. L. Rinnenthal and K.-H. Gericke, J. Chem. Phys. **113**, 6210 (2000).
[40]R. A. Gottscho, R. W. Field, R. Bacis, and S. J. Silvers, J. Chem. Phys. **73**, 599 (1980).
[41]C. Nyeland and G. D. Billing, Chem. Phys. **138**, 245 (1989).
[42]L. K. Cooper, A. J. McCaffery, and S. D. Bosanac, Chem. Phys. Lett. **167**, 233 (1990).
[43]M. H. Alexander, Chem. Phys. **92**, 337 (1985).

[44]M. H. Alexander and H. J. Werner, J. Chem. Phys. **95**, 6524 (1991).
[45]M. H. Alexander and S. L. Davis, J. Chem. Phys. **78**, 6754 (1983).
[46]T. J. Price, Ph.D. dissertation (Lehigh University, 2017).
[47]T. J. Price, A. C. Towne, D. Talbi, and A. P. Hickman, Chem. Phys. Lett. **645**, 180 (2016).
[48]T. J. Price and A. P. Hickman, J. Chem. Phys. **148**, 074105 (2018).
[49]G. Herzberg, *Molecular Spectra and Molecular Structure I, Spectra of Diatomic Molecules* (Van Nostrand Reinhold, New York, 1950).
[50]S. J. Silvers, R. A. Gottscho, and R. W. Field, J. Chem. Phys. **74**, 6000 (1981).
[51]L. D. Snow, R. N. Compton, and J. C. Miller, J. Chem. Phys. **88**, 1652 (1988).
[52]G. Sha, W. Sun, B. Jiang, E. Hintsa, and C. Zhang, J. Chem. Phys. **98**, 9487 (1993).
[53]R. B. Kurzel and J. I. Steinfeld, J. Chem. Phys. **56**, 5188 (1972).
[54]S. R. Jeyes, A. J. McCaffery, M. D. Rowe, P. A. Madden, and H. Katô, Chem. Phys. Lett. **47**, 550 (1977).
[55]C. R. Vidal and J. Cooper, J. Appl. Phys. **40**, 3370 (1969).
[56]W. Demtröder, *Laser Spectroscopy: Basic Concepts and Instrumentation* (Springer, 2003).
[57]A. N. Nesmeyanov, *Vapor Pressure of the Chemical Elements* (Elsevier Publishing, New York, 1963).
[58]H. Chen, L. Li, G. Lazarov, X. Wang, A. M. Lyyra, J. Huennekens, and R. W. Field, J. Mol. Spectrosc. **196**, 197 (1999).
[59]R. Stair, W. E. Schneider, and J. K. Jackson, Appl. Opt. **2**, 1151 (1963).
[60]E. U. Condon and G. H. Shortley, *The Theory of Atomic Spectra* (Cambridge University Press, 1964).
[61]J. Pitre and L. Krause, Can. J. Phys. **46**, 125 (1968).
[62]A. C. G. Mitchell and M. W. Zemansky, *Resonance Radiation and Excited Atoms* (Cambridge University Press, London, 1971).
[63]A. Sanli, X. Pan, D. S. Beecher, S. Magnier, A. M. Lyyra, and E. H. Ahmed, J. Mol. Spectrosc. **355**, 1 (2019).